N70-15606
NASA-CR-73402

UNCLASSIFIED

NASA CR 73402
AVAILABLE TO THE PUBLIC

# CARBON-14 RADIATION DETECTION SYSTEM FOR LIFE DETECTION EXPERIMENTS

By Benton C. Clark

November 1969



Prepared under Contract No. NAS 2-5547 by
AVCO ELECTRONICS DIVISION
Tulsa, Oklahoma

for

AMES RESEARCH CENTER

NATIONAL AERONAUTICS AND SPACE ADMINISTRATION

ACKNOWLEDGEMENTS

This investigation was conducted in the Radiation Instrumentation Laboratory at Avco/Tulsa under the technical direction of Dr. B. C. Clark. Valuable contributions to the success of the investigation were made by A. A. Sanders and C. W. Bennett. We wish to thank Dr. D. Srdoc of the Institute Ruder Boskovic, Zagreb, Yugoslavia, for important suggestions on the design and operation of the spherical proportional counter.

## ABSTRACT

A carbon-14 radiation detection system has been developed for use in a science breadboard experiment to demonstrate the feasibility of detecting life on Mars using the $^{14}CO_2$ tracer technique. The detection system consists of a spherical proportional counter to measure the beta rays from $^{14}C$. This counter is built inside a plastic scintillator. Pulses from the photomultiplier tube which views this scintillator and from the wire anode of the proportional counter are amplified and fed to an anti-coincidence circuit which passes the proportional counter pulses only when no pulse occurs in the scintillator. The purpose of the scintillator and anti-coincidence circuitry is to reduce sensitivity to background radiation, especially that produced by the SNAP-19 units in the radioisotope thermoelectric generators (RTG's) planned for use on the Viking Lander. Two carbon-14 radiation detection systems have been fabricated and optimum operating characteristics defined. Tests performed with a SNAP-19 unit have demonstrated that the anti-coincidence effectiveness factor of the system is as high as 30 for SNAP-19 radiation. Under optimum operating conditions, the detection system achieves a figure of merit of 6.2 in the presence of the SNAP-19 and 27 in the laboratory environment. This allows lower limits of detectability of 7 picocuries and 1.4 picocuries of $^{14}CO_2$, respectively, at a confidence level of 0.999999. The detection system can reliably measure all activities between the quoted lower limits up to and greater than 2.5 microcuries of $^{14}CO_2$.

Other tests performed on the system included effects of gas pressure and composition variations, comparison of gas flow vs. batch operation, memory effects and determination of voltage bias effects, detection efficiency for $^{14}CO_2$, and reproducibility of measurements. In addition, data has been obtained relative to the special requirements of the Viking mission, including variation of operating temperature, presence of water vapor, power consumption, and exposure to sterilization procedures.

As a result of these studies, methods of reducing the radiation interference from the RTG's are recommended in terms of location, orientation, shielding, and manufacturing procedures for the SNAP-19. Areas requiring further investigation include the study of a cesium iodide scintillator and a flight-qualified photomultiplier tube, design of the system for withstanding all sterilization and mechanical stress environments, and development of countermeasures to the effects of water vapor and electro-negative gases upon the operation of the system.

TABLE OF CONTENTS

TABLE OF CONTENTS
(Continued)

## 1.0 INTRODUCTION

The exploration of Mars by the NASA Viking spacecraft will include experimental studies by both the orbital and lander portions of the probe. One objective of the lander spacecraft will be to conduct experiments on the Martian surface which seek to detect the existence of native life. Present goals are to search for carbon-based life. This allows the use of carbon-14 ($^{14}C$) as a radioactive tracer.

The search for life must, of course, employ instruments which have the highest practical sensitivity in order to detect low levels of life or to determine an upper limit to the degree of life present. They also must have a large dynamic range to cover the possibility of the presence of relatively high levels of biological activity. This implies that the $^{14}C$ detection system must be capable of detecting and quantifying very low to very high levels of $^{14}C$. Accurate measurement of low levels of the radioisotope will be difficult because of interference by natural environmental radiation and radiation produced by on-board radioisotopic thermoelectric generators (RTG's).

The basic requirement of this work is to consider all mission constraints and environments, sensitivity levels, and operating range, and to design $^{14}C$ detection equipment which will produce optimum results for this application. The detection equipment must be small, lightweight, and rugged. Because of its importance to the mission, it must be highly reliable.

The requirement for detecting extremely low levels of $^{14}C$ dictates the use of a system having the highest practical efficiency for detecting beta rays emitted from $^{14}C$ samples. In the laboratory, a vast amount of experience in $^{14}C$ detection has established the superiority of gas-filled proportional counters over all other types of detection systems for nearly all low-level $^{14}C$ experiments. This is chiefly because (1) the achievable geometric factor is near the theoretical maximum of 1.0, and (2) the superior resolution and signal-to-noise ratios achievable at energies less than a few tens of keV allows discriminate detection of even the lowest energy beta particles emitted by $^{14}C$.

## 2.0 DESIGN

The design of the carbon-14 detection system is based in large part upon the knowledge that it will be necessary to discriminate to the fullest extent possible against the radiation produced by the radioisotope thermoelectric generators (RTG's) on the lander. The detection system consists of a spherical proportional counter surrounded by a plastic scintillator whose output is operated in anti-coincidence with the counter output (a similar system has been tried before, Hu-67*). The conventional approach to rejecting gamma ray background is to make the scintillator very large and of high Z material in an effort to assure that most of the external gamma rays interact at least once in the scintillator. The present approach does not require a high percentage of the gammas to interact with the scintillator. The present approach is based, rather, upon the fact that most of the counts recorded by a proportional counter placed in a gamma ray field are due to electrons ejected from the wall of the counter, while only a small percentage of the counts are due to interactions of the gamma rays with the counter gas. Thus, if the wall material is also sensitive to radiation, those electrons created in the wall can be rejected electronically through the anti-coincidence technique. When the counter is filled with carbon-14 labelled gas, some of the beta rays from the carbon-14 can also enter the wall material and thus produce counts in the scintillator guard. By varying the discriminator threshold of the scintillator system through electronic means, it is possible to optimize the response

---

* References are listed in section 7.0.

of the anti-coincidence system so as to minimize losses of carbon-14 counts and maximize background rejection.

The detector volume is selected to be a nominal 30 cc, based on estimated sample size. This is achieved with a 1.5" diameter spherical detector.

A number of advantages are gained by employing a spherical proportional counter in this application, instead of the more conventional cylindrical counter. It should be pointed out that one chief reason for the widespread use of cylindrical counters is their relative ease of fabrication, especially where economic factors have a strong influence in design of instruments to be used commercially. However, the special requirements of the Viking $^{14}C$ detection system readily justify the additional effort necessary to employ a spherical device. Some of the advantages of a spherical counter versus a cylindrical counter are: (1) achieves minimum possible weight for a given sensitive volume, (2) a larger fraction of the total counter volume is sensitive to radiation, (3) provides maximum efficiency in collecting light signals in the anti-coincidence shield, and (4) offers greater suitability for gas flow purging technique because there are no stagnation areas. These advantages are discussed in detail in the succeeding paragraphs.

The sphere has the smallest surface area for a fixed total volume of any shape. Thus, for a selected amount of shielding in terms of $g/cm^2$, the least total weight is required. This is vividly demonstrated by the comparison of a cylindrical and spherical counter shown in Figure 1. In this figure, both counters have a total volume of 30 $cm^3$. However, as shown in the accompanying table of calculations, approximately 50% more weight is required to shield the cylindrical counter than is required for the same thickness of shielding around the spherical counter. For aerospace application, the spherical counter is clearly superior in this respect.

Less "dead volume" exists in spherical counters than in cylindrical counters. This volume is composed of regions inside the counter from which charge cannot be collected on the center wire. In cylindrical counters, these regions exist at the corners defined by the end plates and cylindrical surface. It is usual practice to employ field tubes in cylindrical counters to shape the field near the end plates. That portion of the wire surrounded by the field tubes is insensitive to radiation produced outside the tubes. In typical cases, a cylindrical device has dead volume ranging from 20 to 40% of the total volume. Thus, the sensitive volume to be expected for a cylindrical counter is about 80%, whereas in a spherical counter, a sensitive volume equal to 95% or more of the total volume is not difficult to achieve.

Collection of light generated in the scintillator by radiation is much more efficient in a spherical detector than a cylindrical one. As seen in Figure 1, the maximum distance between any point in the scintillator material and the phototube is only 1.5 inches for the spherical geometry, whereas it reaches 4.0 inches in the cylindrical configuration. The greater distances in the latter case will diminish the sensitivity of the scintillator-photomultiplier system and thereby

Scale: Actual Size

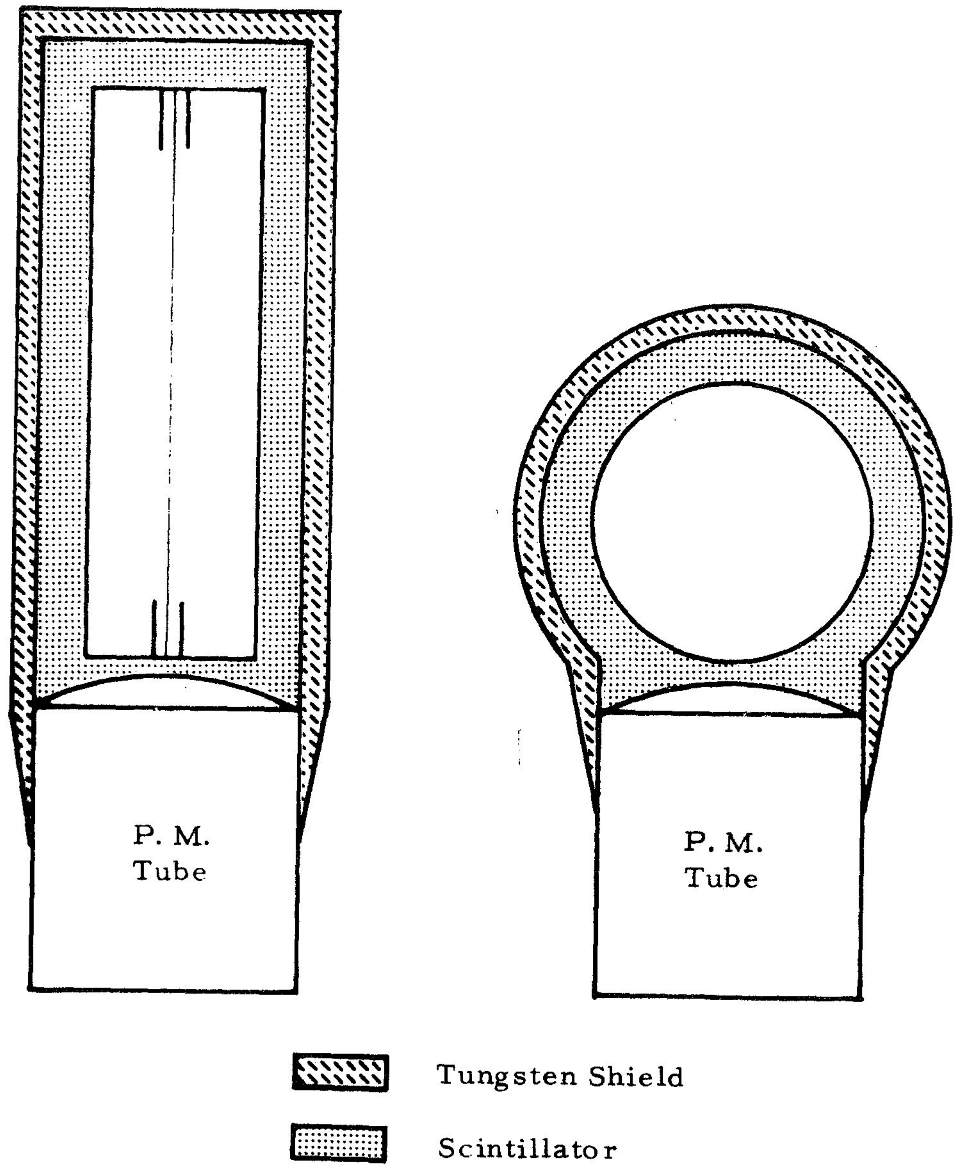


| | Cylindrical Counter | Spherical Counter |
|---|---|---|
| Inside Diameter | 0.87 inch | 1.50 inch |
| Inside Length | 3.0 inch | N. A. |
| Scintillator Weight | 0.15 pounds | 0.10 pounds |
| Tungsten Weight | 1.56 pounds | 1.07 pounds |

Figure 1. Comparison of Size and Weight of Cylindrical and Spherical Counters.

reduce the efficiency of the anti-coincidence circuit in reducing background counts.

If a gas flow method is employed to flush the chamber between samples, the spherical chamber may be more suitable for this approach. This is because the corner areas near the end plates of a cylindrical counter are areas at which stagnation or inadequate mixing can occur between input gas and resident gas, resulting in streaming between inlet and outlet tubes.

The counter system is shown in Figure 2. The relative geometry selected for the spherical counter comes from the experimental work of Benjamin et al (Be-68). A thin stainless steel wire is fixed by two feedthrough insulators with metal bosses on the inside for positioning the wire and also to provide shaping of the electric field at this location in the counter. The pressed-fit caps on the opposite ends of the feedthrough insulators are used to anchor the wire and to provide an edge which can be soldered to seal the tubes of the inserts. Although it is highly desirable that a flight unit incorporate a wire held under spring tension, it was not found necessary in the present work to incorporate a spring at the end of the wire.

The scintillating material selected is an organic material (a phosphor solution in polyvinyltoluene) sold under the trade name NE-160 (Nuclear Enterprises, Ltd., San Carlos, California). This scintillator is especially compounded for use at high operating temperatures (up to 150$^{\circ}$C). For simplicity and ease of construction, the external shape of the scintillator is made cylindrical, while the internal cavity is spherical with two cylindrical cavities for mounting the feedthrough insulators.

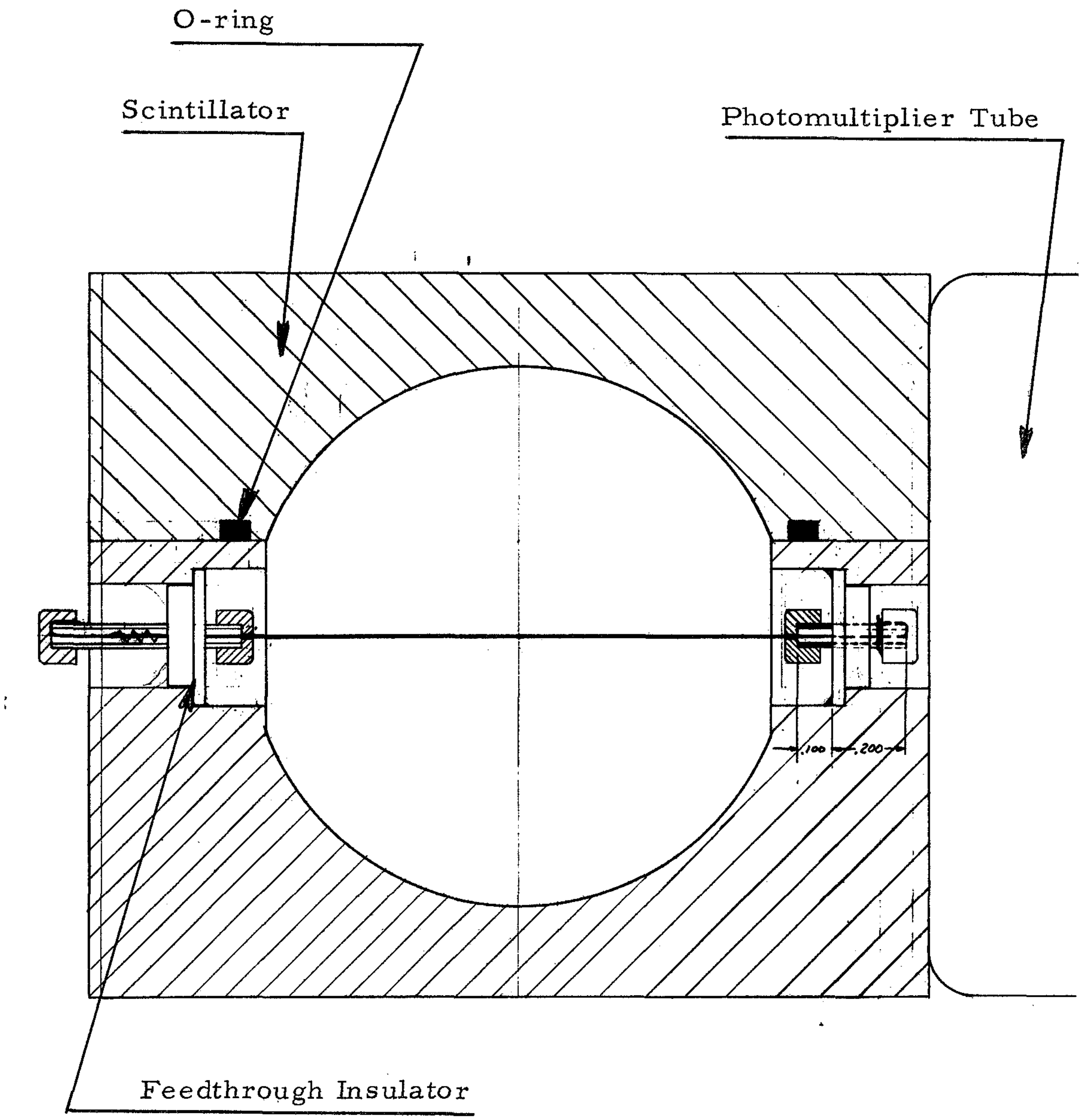


Fig. 2. Cross-section schematic of the carbon-14 detection system showing spherical proportional counter inside a cylinder of plastic scintillator which is optically coupled to the face of a photomultiplier tube. Gas-flow tubes are not shown. See text for additional description. Scale = twice actual size.

All internal surfaces of the machined scintillator parts are metallized by vacuum coating with aluminum. This is important for three reasons: (1) to provide a conductive coating for the cathode connection, (2) to seal the plastic from the radioactive gas in order to minimize absorption of the gas and outgassing of electro-negative gases dissolved in the plastic, and (3) to provide a light barrier between the gas and the scintillator material so that gas scintillations will not be detected.

The feedthrough inserts and brass gas-flow tubes are epoxied to the scintillator using NE-580 optical cement. Vacuum coating is performed after installation of these items, but prior to installation of the wire. An O-ring of Viton-A seals the chamber when the two halves of scintillator material are forced together by an aluminum clamp. The assembled and disassembled detection system is shown in Figures 3 and 4. The exterior surface of the scintillator is coated with titanium oxide paint for maximum reflectivity. One end of the cylindrical assembly is coated with a silicone grease (Dow-Corning No. 20-057) and mated to the photocathode face of an end-window photomultiplier tube. This tube is mounted in a special photomultiplier housing assembly, Model E-258, manufactured by EMI/Varian Corporation, Plainview, New York. A deep drawn steel can with a MHV connector for the proportional counter anode and feedthroughs for the two gas-flow tubes is mounted to this assembly to provide a light-tight, electrostatic shield around the scintillator.

As will be discussed below in the section on sterilization compatibility, the use of NE-160 plastic scintillator produces problems in maintaining dimensional stability under high temperature bake

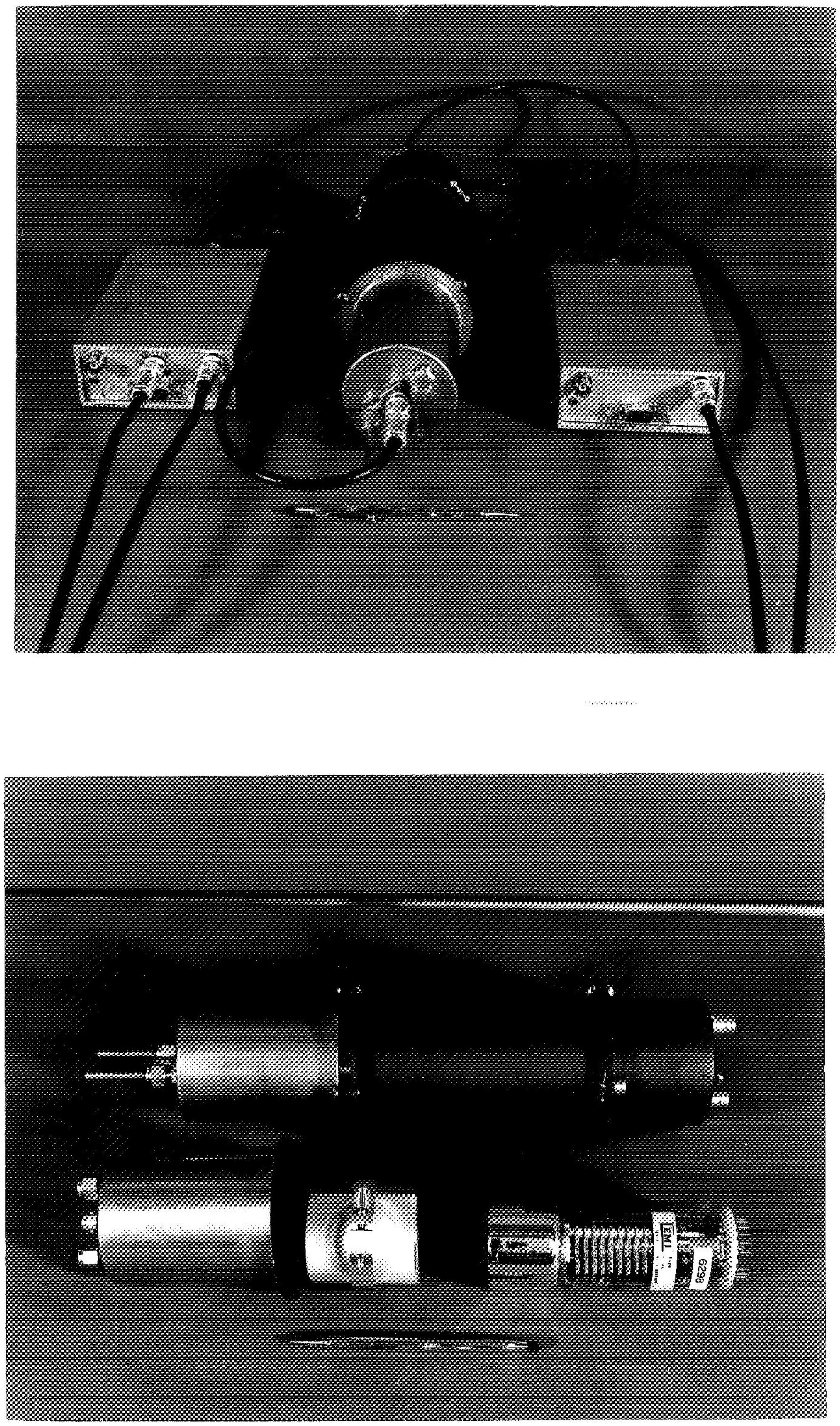

Fig. 3. The carbon-14 detection system. Top view, fully assembled and connected to preamplifiers. Bottom view, disassembled showing the scintillator-proportional counter and photomultiplier tube.

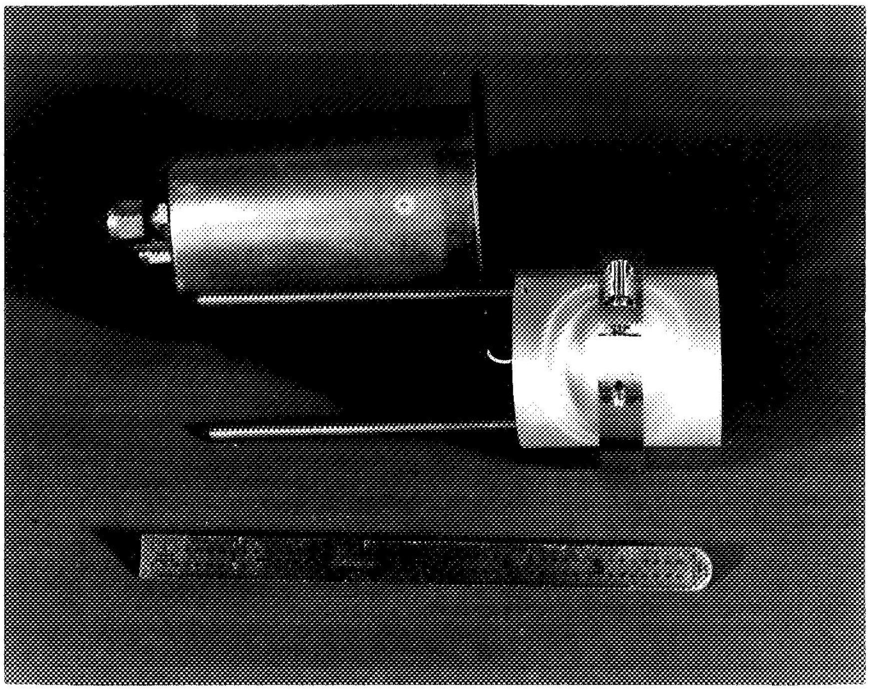

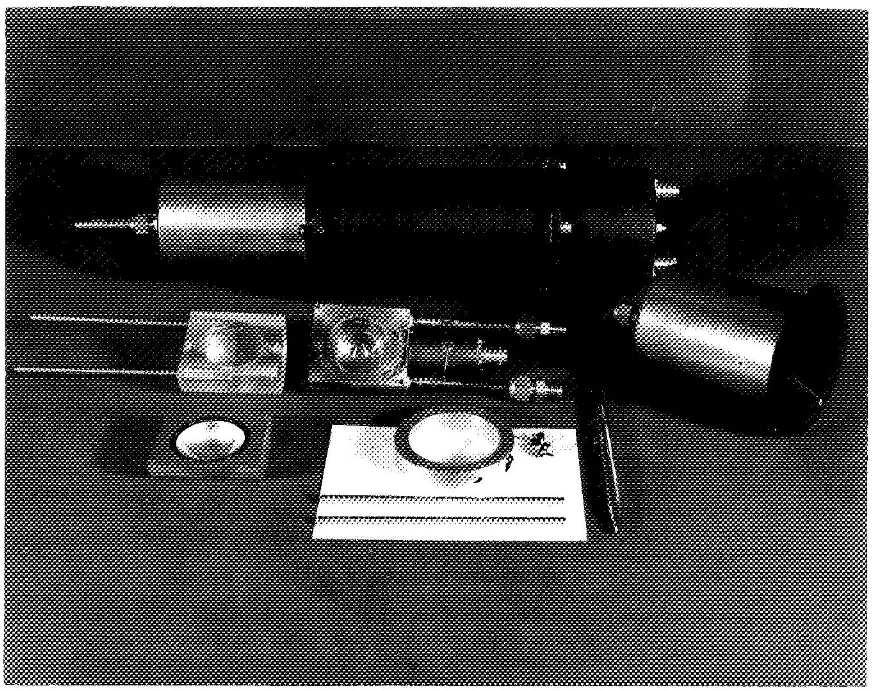

Fig. 4. The carbon-14 detection system shown in various stages of disassembly.

conditions. In an effort to obtain a scintillator which would be very resistant to heat, we sent letters to twelve possible vendors soliciting a quotation on the manufacture of a cesium iodide scintillator in the required shape. None responded in the affirmative. However, special circumstances prevented one vendor (Harshaw Crystal Division) from quoting, whereas at a later date they should be able to supply this item.

In Table I, details of construction peculiar to systems #1 and #2 are given. Otherwise, these detection systems are identical.

Table I. Differences in Construction Details for Detection Systems #1 and #2

| Feature | Detection System #1 | Detection System #2 |
|---|---|---|
| Diameter of wire in proportional counter (mils) | 2.5 | 1.0 |
| Type of photomultiplier tube (EMI model number) | 9727B | 9635B |
| Photocathode (bialkali) | SbKNa | SbKCs |
| Maximum storage temperature | 150°C | 80°C |

## 3.0 EXPERIMENTAL METHODS

The electronic equipment required for operating the carbon-14 detection system is outlined in the block diagram, Figure 5. The actual equipment used is listed by model and manufacturer in Table II. A special resistor network is built into the base of each photomultiplier tube assembly and a schematic of this network is given in Figure 6. The preamplifier employed for the proportional counter is of the charge-sensitive type with an output of 500 millivolts/picocoulomb. The preamplifier employed for the photomultiplier tube is similar, producing 3.3 millivolts/picocoulomb. In the Geiger counter mode of operation the photomultiplier preamplifier was employed with the counter as shown by the arrangement of Figure 7.

A photograph of the electronics and gas flow system with one of the units connected is shown in Figure 8. The gas handling apparatus is a slightly modified system originally built by Avco for use in the study of space-qualified proportional counter systems. It employs a Model 36-541-09 flowmeter and a Model 6A cartesian manostat, both manufactured by the Manostat Corporation, New York. A gas mixing reservoir allows the compounding of special mixtures. Composition is determined in terms of percent partial pressure with the aid of a precision vacuum gauge (Ashcroft 1850).

The pumping system is protected by a liquid nitrogen cold finger and a molecular sieve trap, which also prevents loss of radioactive gas to the atmosphere during pumping. Upon completion of an experiment the liquid nitrogen is removed from the cold finger and nitrogen gas at one atmosphere is flowed through the system and into a potassium

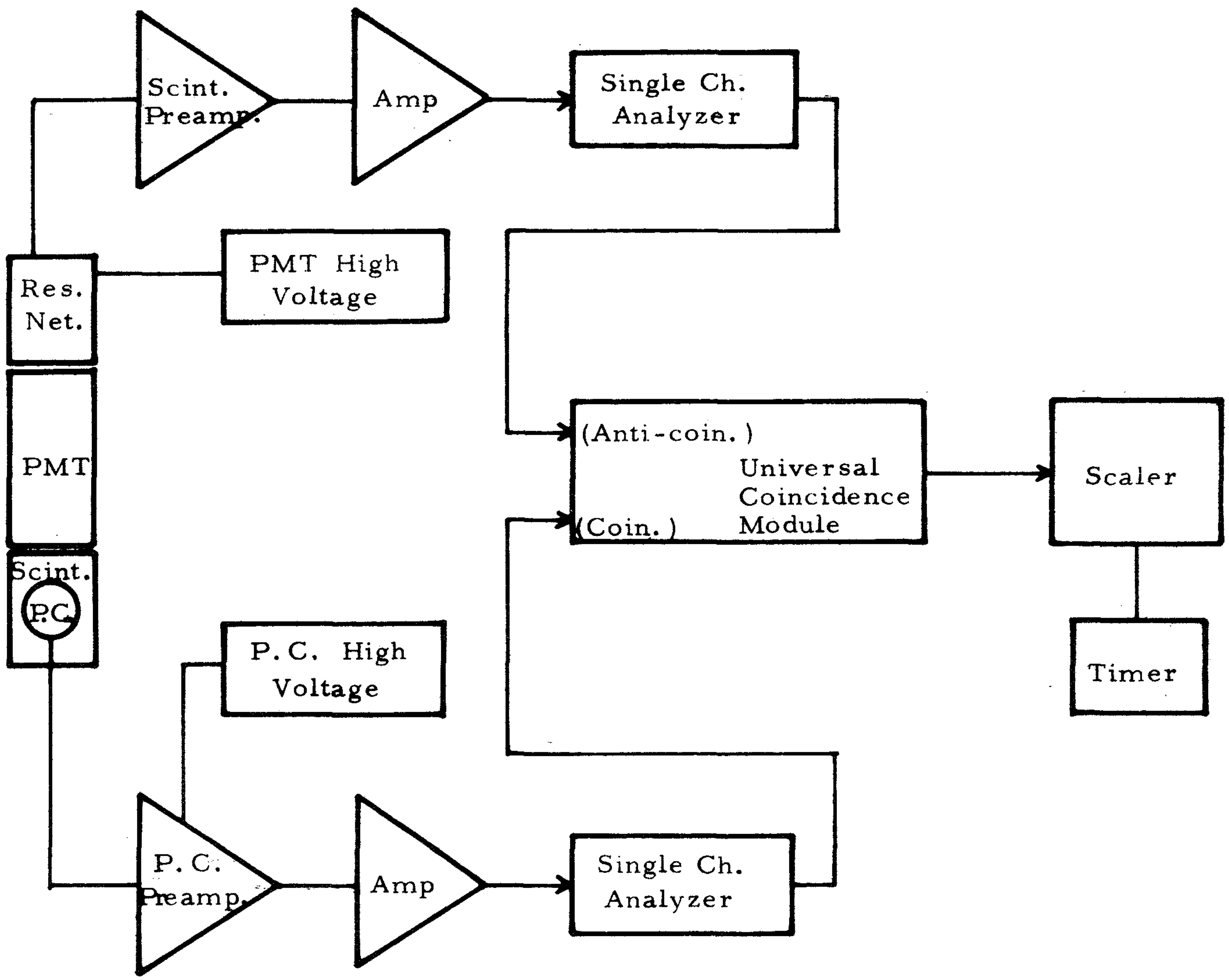


Fig. 5. Block diagram of the electronic equipment used to operate the carbon-14 detection system. See Table II for a list of equipment by manufacturer.

Table II. List of Electronic Equipment Shown in the Block Diagram (Fig. 5).

Res. Net. - Resistor network used to bias the dynodes of the photomultiplier tube. See Fig. 6 for details.

Scint. Preamp - Canberra* Model 1405

Amp - Canberra Model 1418

PMT High Voltage - Fluke** Model 405B

Single Ch. Analyzer - Canberra Model 1431

Universal Coincidence Module - Canberra Model 1446

Scaler - Ortec*** Model 484

Timer - Ortec Model 482

P. C. High Voltage - Fluke Model 408B

P. C. Preamp - Canberra Model 1406

* Canberra Industries, Middletown, Conn.

** John Fluke Manufacturing Company, Inc., Seattle, Wash.

*** Ortec, Inc., Oak Ridge, Tenn.

R = 110 K

$C_1$ 0.01, 1 KV

$C_2$ 0.001, 3 KV

ZD = 1N3051A (200 V.)

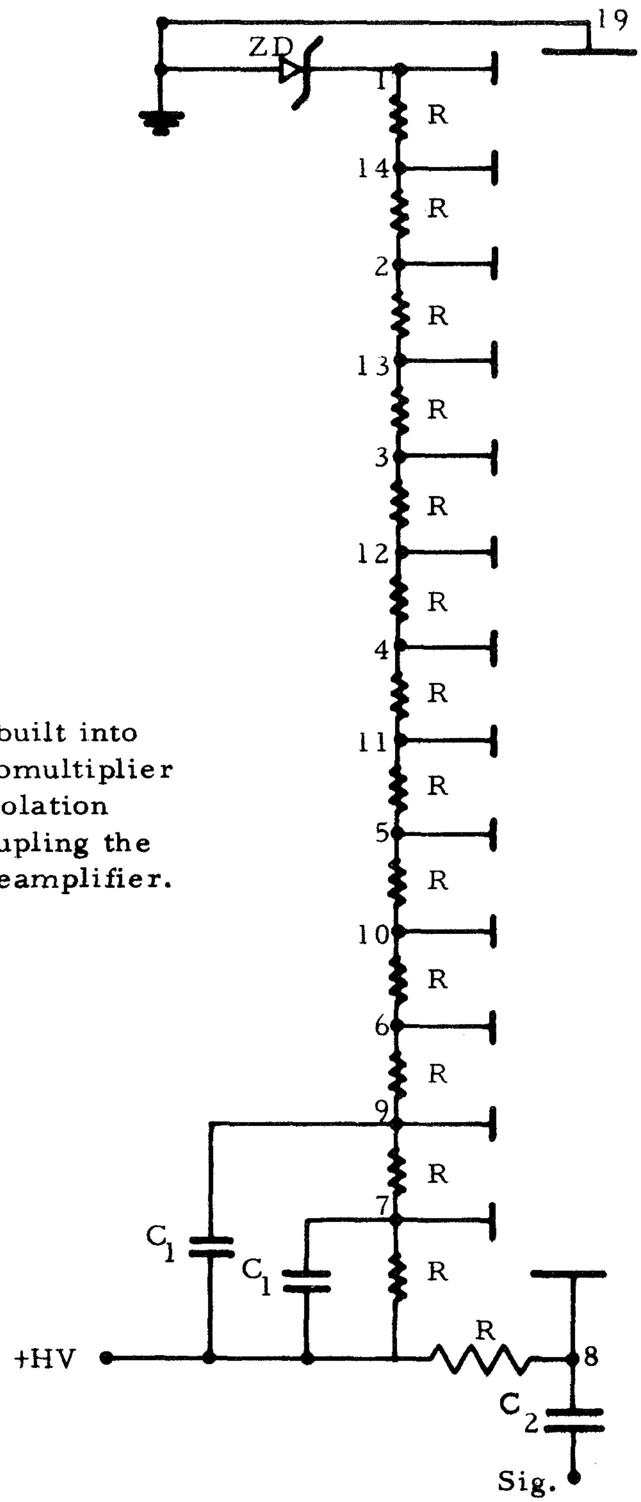


Fig. 6. Electrical network built into the base of the photomultiplier housing, showing isolation capacitor $C_2$ for coupling the output pulse to a preamplifier.

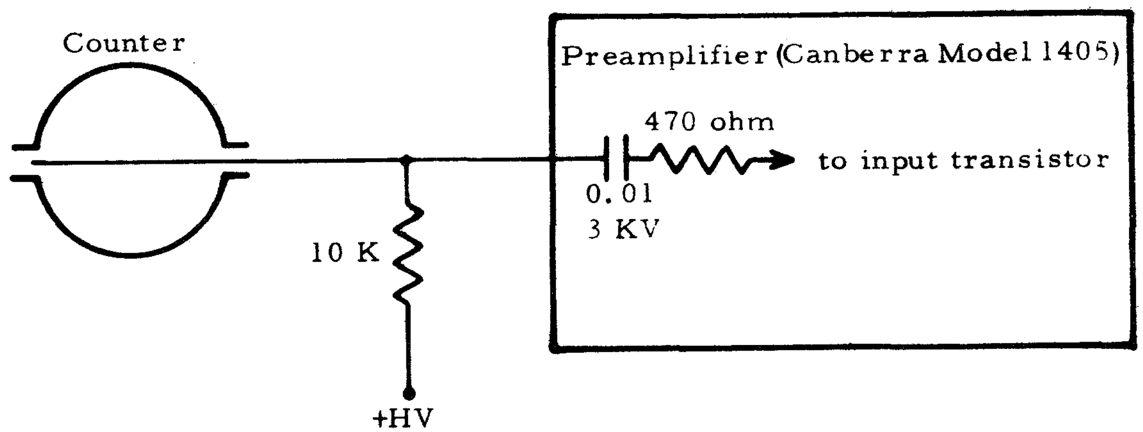


Fig. 7. Schematic of the readout method employed when operating the sensor as a Geiger counter.

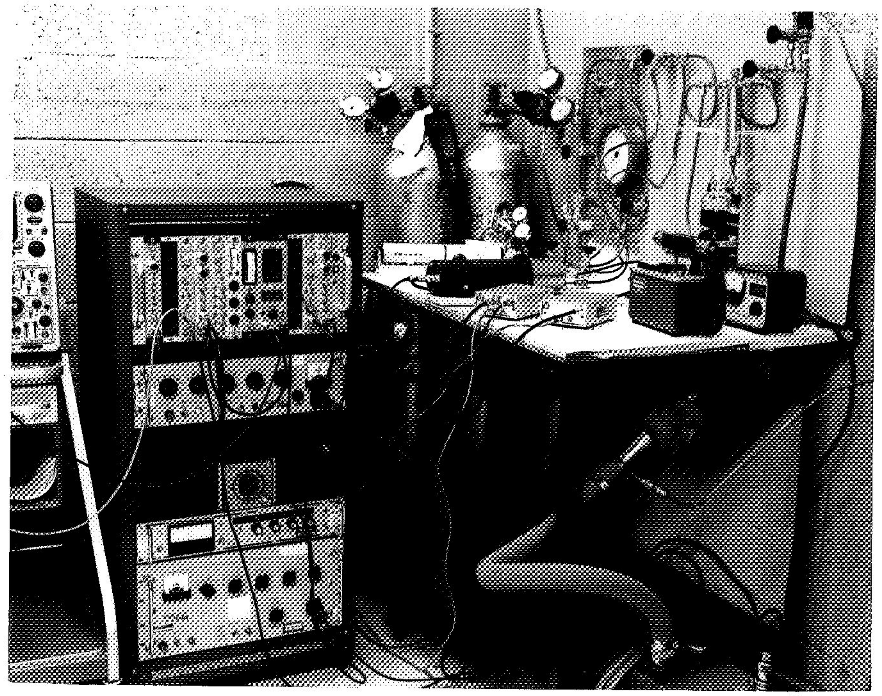

Fig. 8. View of carbon-14 detection system connected to the gas flow system. Also shown are the preamplifiers and the rack of nuclear electronic equipment given in the block diagram of Fig. 5.

hydroxide scrubber. Thus, the radioactive carbon dioxide condensed on the cold finger is allowed to sublimate and then is trapped as a solid waste by formation of a potassium carbonate precipitate in the scrubbing solution. No detectable loss of radioactive gas has been encountered using this system, even with sample activities as high as several hundred microcuries. Radioactive gas was procured from The Matheson Company, Inc., East Rutherford, New Jersey.

## 4.0 EXPERIMENTAL RESULTS

### 4.1 Typical Operating Conditions

A plot of the gas multiplication factor vs. the high voltage bias placed on the proportional counter is shown in Figure 9. The multiplication factor was calculated from the known charge sensitivity of the preamplifier and the known energy deposition of the source radiation employed (5.9 keV). This source was an iron-55 soft x-ray emitter which entered the counter through a 1.0 mil beryllium window. Both counter #1 with a 2.5 mil center wire and counter #2 with a 1.0 mil center wire were studied. The gas was 90% argon, 10% methane (P-10) at a pressure of 0.5 atmospheres. The data show that gas multiplication factors over 30,000 can be reliably achieved with this counter geometry. In most of the data which follows, the proportional counters were operated with gas gains between 1000 and 10,000. Of interest is the relationship between required bias voltage and wire diameter for achieving the same gas gain. Thus, a gain of 1000 is achieved with 1400 volts bias on counter #1, but with only 1070 bias volts on counter #2.

The integral spectrum produced in the counter by carbon-14 is shown in Figure 10. It is noteworthy that less than 10% of the pulses produce an energy greater than 25 keV, even though 10% of the beta rays emitted by carbon-14 have an energy exceeding 100 keV, Figure 11. This is a consequence of the fact that the amount of energy that can be lost by an electron passing straight across the diameter of the counter is only 35 keV for a 0.5 atmosphere filling pressure (Ne-58); thus, very few pulses above this

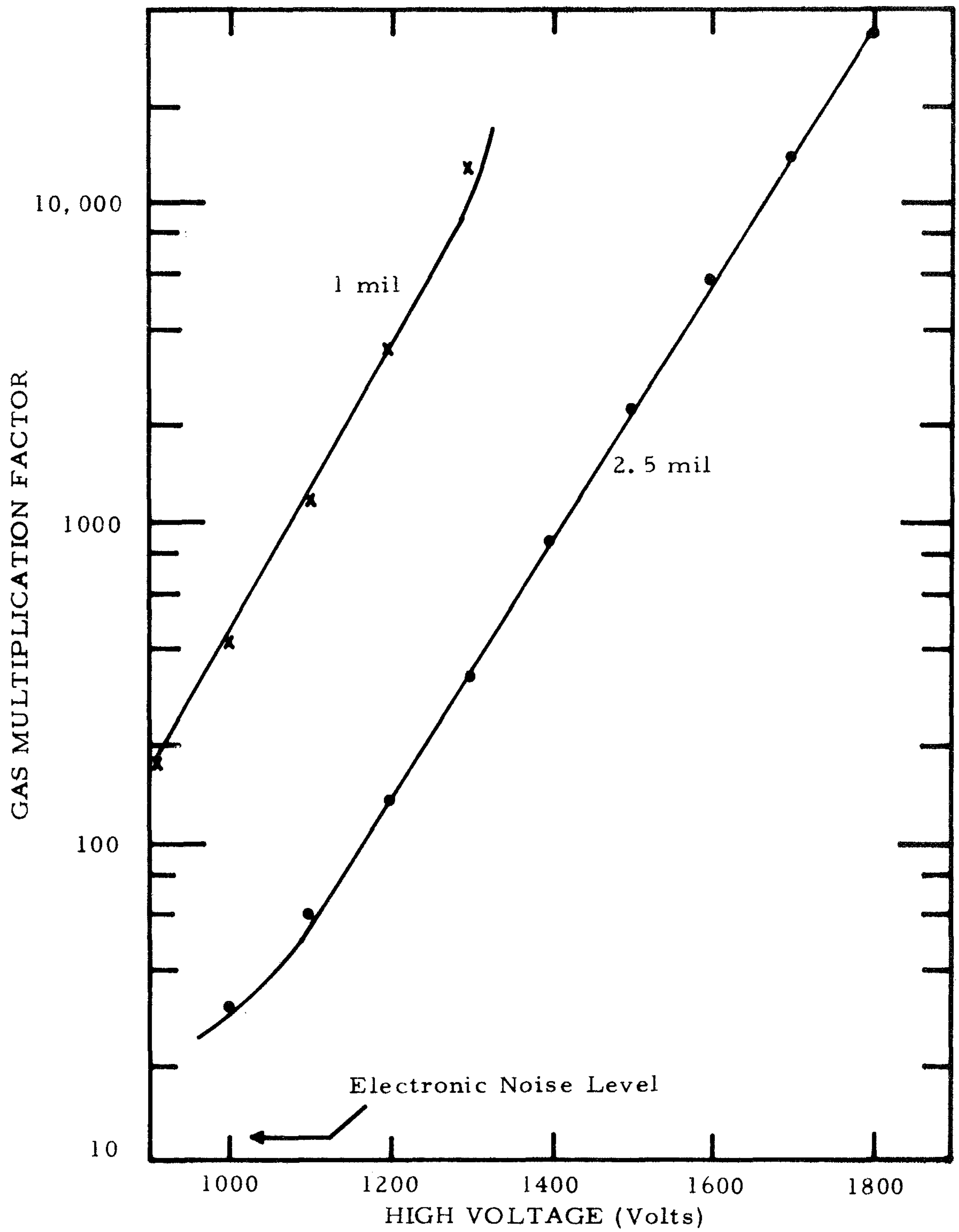


Fig. 9. Gas gain as a function of applied bias for counter #1 (2.5 mil diameter wire) and counter #2 (1.0 mil wire). Gas is P-10.

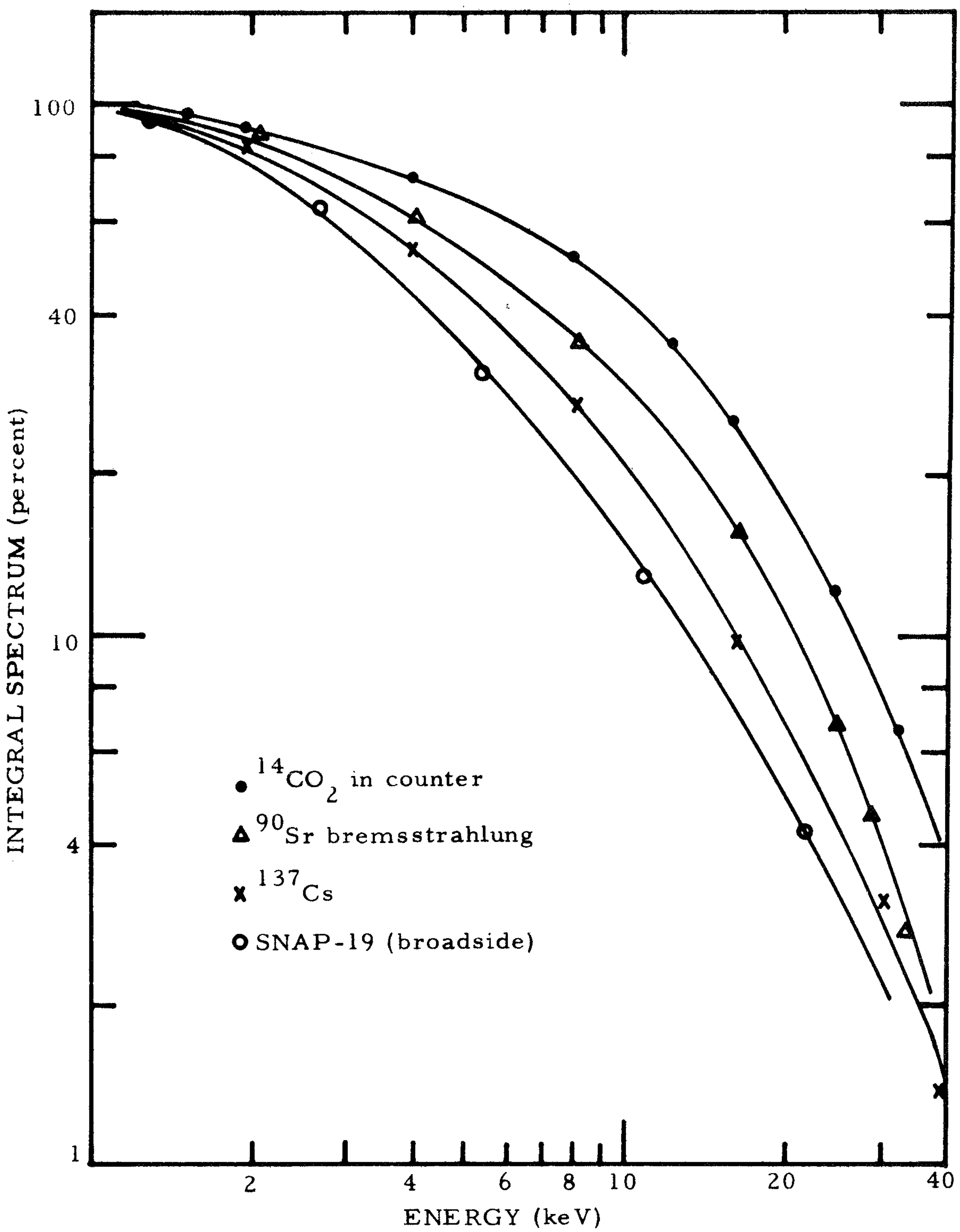


Fig. 10. Integral energy spectra measured in the proportional counter for $^{14}CO_2$, and for various external sources. All spectra have been normalized to 100% at 1.0 keV.

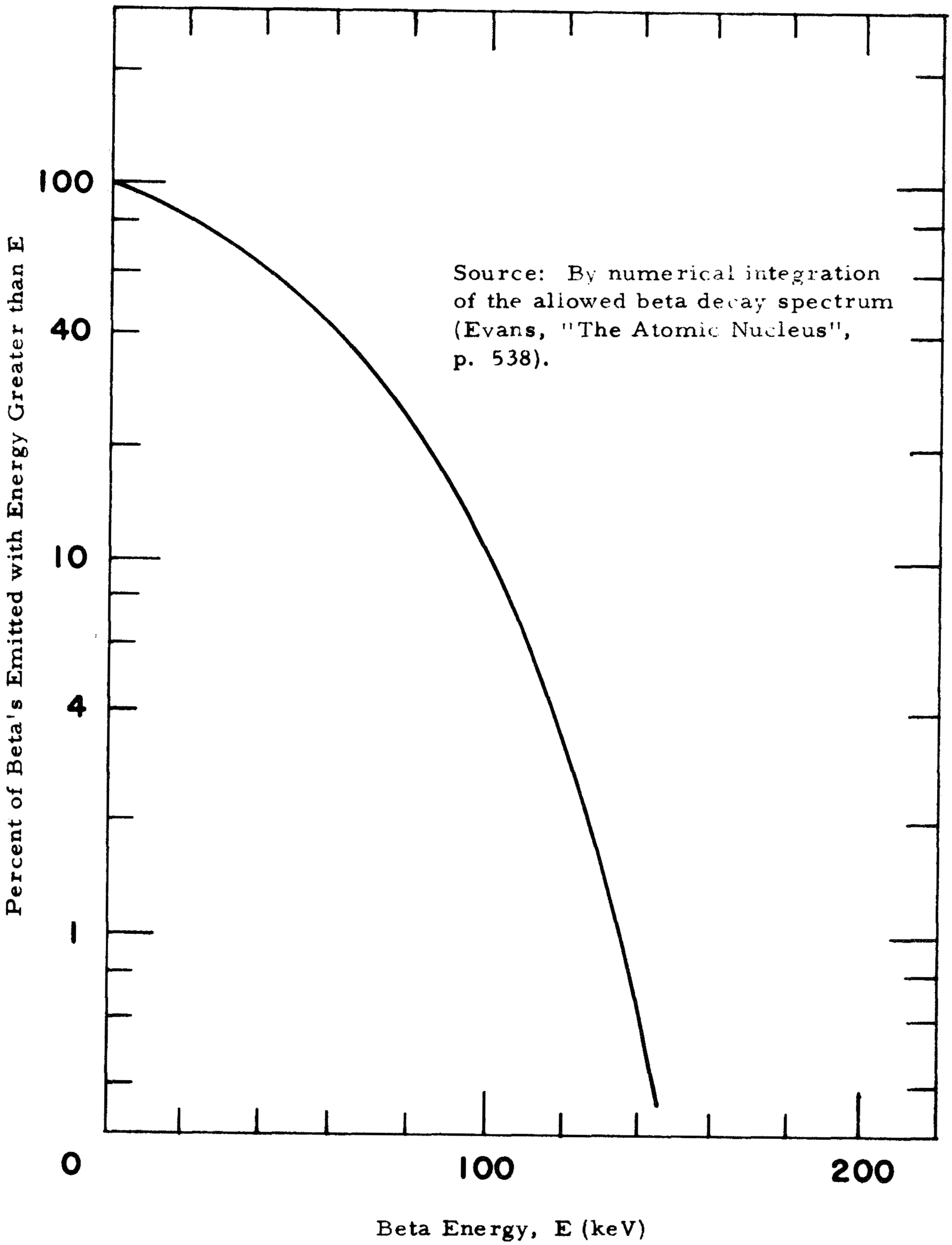


Figure 11. Percent of $^{14}C$ beta particles emitted with energy above E keV.

energy are expected and indeed few are observed. These few are chiefly due, in fact, to electrons which suffer a large amount of scattering as they pass through the counter volume. Integral spectra for three other radiation sources are also shown in Figure 10. All curves have been normalized to 100% at 1 keV energy. It will be noticed that the curves are qualitatively quite similar. Raising the energy threshold provides rejection of a larger percentage of background counts than $^{14}C$ counts, but this is not an effective way to optimize the system, as will be shown in the discussion below. Also noteworthy is that for energies below about 1.5 keV the count rate changes very little, indicating that nearly all events deposit at least this amount of energy in the counter.

## 4.2 Gas Pressure

The variation of the gas multiplication factor with changes in the pressure of the gas filling has been determined by measuring the peak amplitude of the iron-55 pulses. The results are shown in Figure 12 where counter pressure is plotted against relative pulse height produced by the source. As expected, gas gain is strongly dependent upon pressure. The line through the data points follows the equation

$$G = k\,P^{-4.9}$$

where G is the gas gain and P is the absolute pressure in Torr. This means that a 1% fluctuation in gas pressure produces a 4.9% change in gas gain.

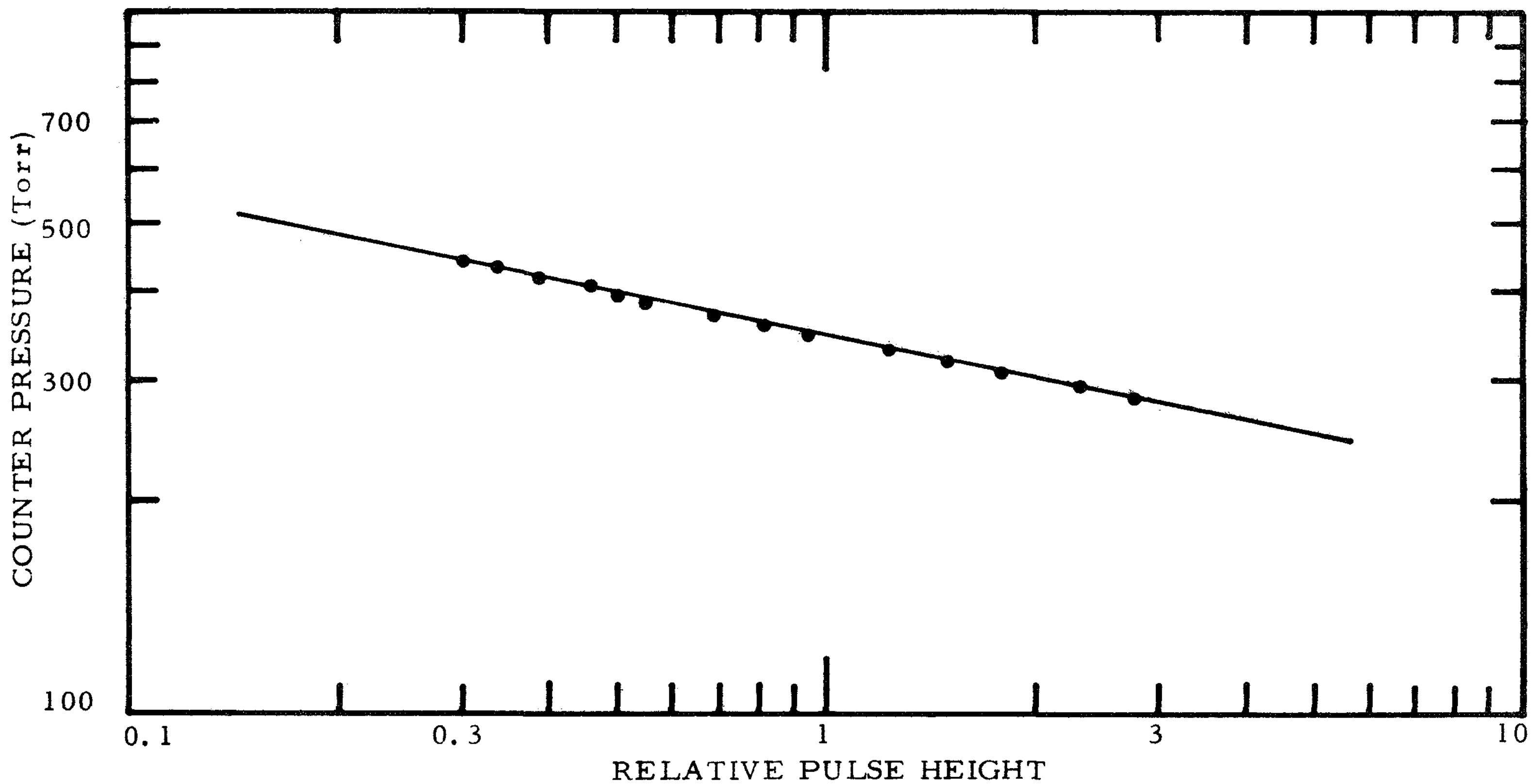


Fig. 12. Sensitivity of gas gain (relative pulse height) to variations in gas pressure. Data taken with counter #1 filled with P-10 gas and operated at 1500 V.

## 4.3 Gas Composition and Quench Gas

The counting gas may be a noble gas to which is added 10% $^{12}CO_2$. Since this gas will be used both in the detector and in a gas chromatograph, it cannot contain constituents which would be removed by the chromatography column.

Of the noble gases, helium has such a low density under standard conditions that its stopping power for the $^{14}C$ beta rays would be unsatisfactory. Krypton is not suitable for low-level counting because of the contamination of commercially-available krypton by the beta emitter, $^{85}Kr$ (Cl-69). Radon is clearly unsatisfactory. The remaining noble gases are neon, argon, and xenon, of which argon is the most conventional choice, the most economical, and should be quite suitable for this application.

Addition of $CO_2$ to either pure argon or an argon-methane mixture significantly reduces the gas gain of the counter. This is shown in Figure 13 where the relative pulse height produced by the iron-55 calibration source is plotted as a function of the carbon dioxide concentration. Data for both argon and P-10 can accurately be described by the equation

$$G = K \exp\left\{ - [CO_2] \; / \; 9 \right\}$$

over the concentration range 0-25% $CO_2$ where $[CO_2]$ is the $CO_2$ concentration in percent by partial pressure. It should be noted that when pure argon or argon with only a trace amount of $CO_2$ is placed in the counter, the pulses produced have a highly variable and irregular shape with a great deal of after-pulsing in evidence.

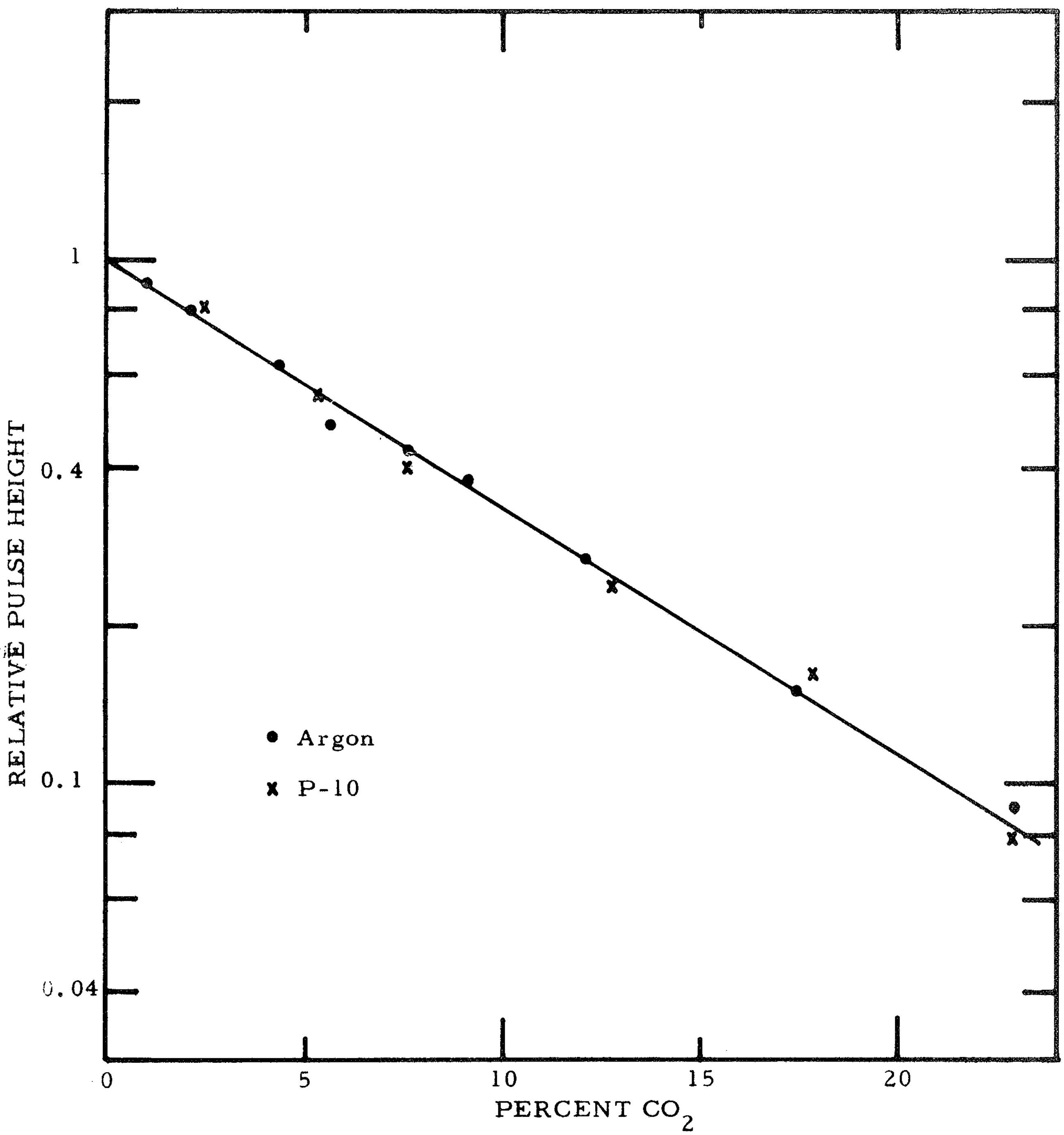


Fig. 13. Sensitivity of gas gain to variations in concentration of $CO_2$. Data taken with counter #1 filled to 0.5 atmosphere and biased at 1500 V.

This is obviously due to the lack of a suitable quenching agent. In general, an argon-$CO_2$ mixture is just as satisfactory as an argon-methane mixture for use in the proportional counter. However, as will be shown below, it is not suitable for use in operating the counter in the Geiger region.

## 4.4 Gas Flow vs. Batch Operation

When a radioactive sample is placed in the counter, and then this sample is flushed with a non-radioactive gas, the count rate will decrease with time according to the formula

$$R = R_o \exp(-t/t_o)$$

where R is the counting rate at time t, $R_o$ is the initial counting rate, and $t_o$ is a characteristic time constant obtained by dividing the counter volume by the gas flow rate. This formula is a theoretical one based upon the assumption that perfect mixing occurs during the flow, i.e., no streaming of the flowing gas directly from the inlet port to the outlet port. Tests were performed at three flow rates: 5, 10 and 20 atmospheric ml/minute. Results for the high and low rates are shown in Figure 14. Here the counter was first filled with 0.34 microcuries of $^{14}CO_2$ mixed with a 90% argon - 10% total $CO_2$ mixture. It can be seen that the decrease in counting rate in each case follows the theoretical time constants of 0.75 and 3.0 minutes quite accurately until the counting rate has decreased by a factor of nearly 2000. At this point, however, the rate of decrease changes drastically. This effect will be discussed in the section on memory effects which follows. It is instructive to compare gas flow operation vs. a batch type operation which includes venting to the Martian

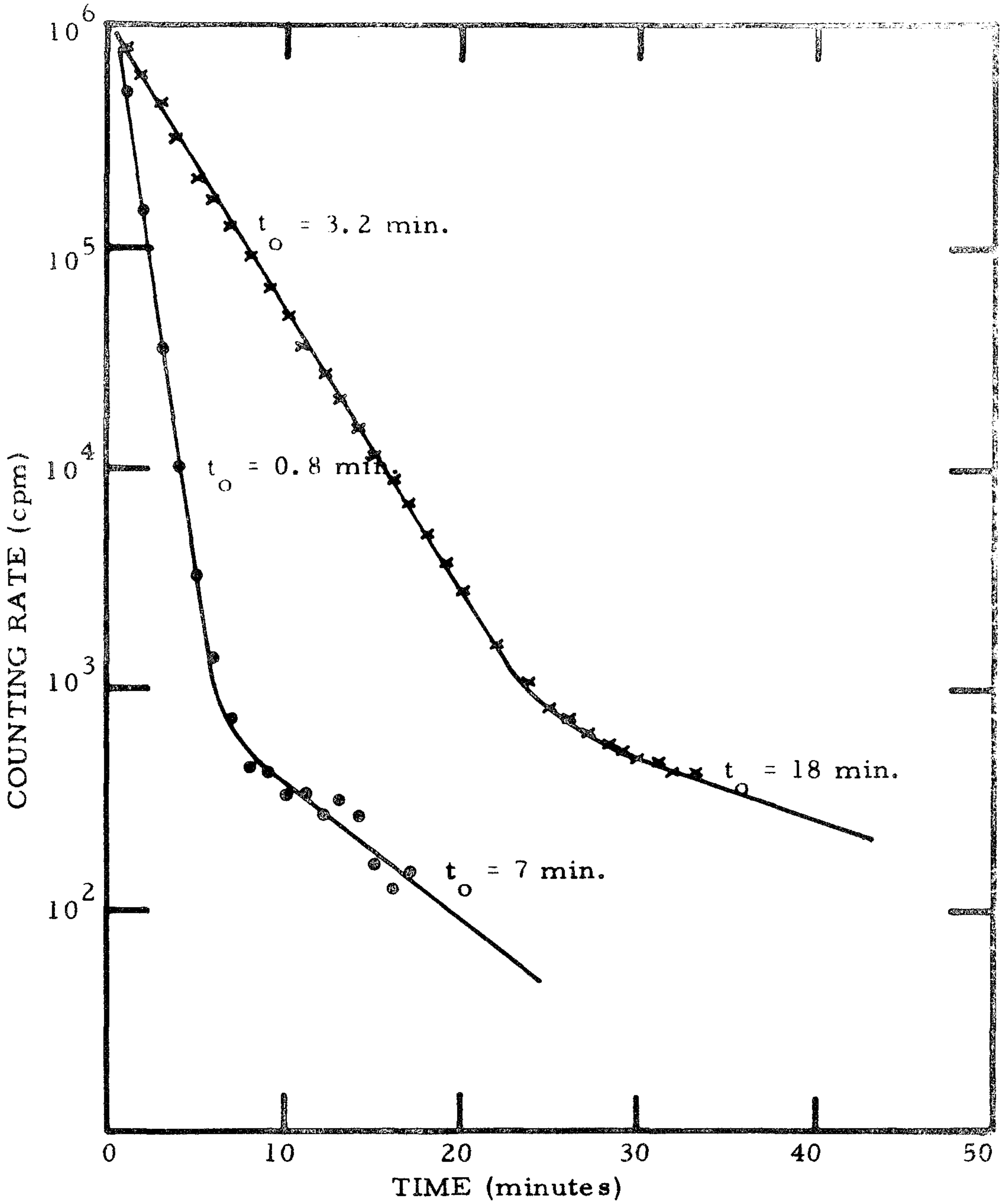


Fig. 14. Decay in counting rate using non-radioactive gas to flush out the carbon-14 sample. Crosses are for a flow rate of 5 atmospheric ml per min., dots are 20 ml/min. See text for discussion.

atmosphere. To simulate the batch operation the counter was filled to a similarly high level of $^{14}CO_2$ activity and the counter allowed to vent to a pressure of approximately 5 millibars. The counter was refilled to approximately 500 millibars pressure (0.5 atmosphere), then vented again to the 5 millibar pressure. The reductions in counting rate achieved by this batch type operation are given in Table III, along with the amounts of gas required for the batch and gas flow modes of operation to achieve a count rate reduction factor of 1000. It is obvious from this data that much less gas is required to achieve the same reduction in count rate using the batch method of operation.

### 4.5 Memory Effects

It is desirable that the counter be capable of analyzing samples in sequence after an intermediate flushing period such that the residual count rate due to the first sample is negligible in the count of the second sample. The design goal is that the residual count rate be $10^{-5}$ of the first sample count rate. As seen in Figure 14, following the initial fast decay in counting rate, the residual decay is very slow. Presumably there is a second component of the original radioactivity which has a long life in the counter and amounts to approximately 0.05% of the original sample. This could be accounted for in two ways: (1) A tiny amount of gas may be semi-trapped inside the small tubes of the feedthrough insulators. This is possible because the internal bosses which support the wire have a very small opening (13.5 mils) which may provide a sufficient impedance that free mixing of the flowing stream

Table III. Comparison of Gas Flow and Batch Operation for Changing Samples (reducing original count-rate by a factor of 1000)

| Mode | Time Required (min.) | Amount of Gas Required (atmospheric ml) |
|---|---|---|
| Gas Flow, 5 ml/min. | 23 | 115 |
| Gas Flow, 20 ml/min. | 6 | 120 |
| Batch* | 2 | 30 |

* Batch operation consisted of venting the sample to 5 millibar (mb) pressure, refilling to approximately 500 mb, venting to 5 mb, and finally refilling to 500 mb to take the final count, which turned out to be 0.0012 of the original count.

with these tiny reservoirs is not possible (the net volume of these two reservoirs is 0.021 $cm^3$, or 0.07% of the counter volume). (2) Radioactive gas absorbed in the scintillator material (Bo-67) could be released back into the counter at a very slow rate. In order to distinguish between these two possible effects, the gas in the counter was completely evacuated following the onset of the slow decay rate. The counter was then filled with non-radioactive gas to the original pressure and the count resumed. In all cases this reduced the counting rate by approximately one-half, but did not reduce it to the original background level. Further pumping (overnight) and refilling with the cold gas reduced the counting rate by an additional factor of 5. Thus, apparently both mechanisms are operative, with the original reduction by half being chiefly due to a small trapped volume of gas within the counter which can be removed by pumping but which does not freely mix with the gas flow, and the residual activity being due to sample that has diffused into the scintillator material. It is believed that performance can be improved with respect to both effects. In the case of the trapped volume, this can be minimized much further by inserting capillary tubing into the feedthroughs to minimize the effective trapping volume. Also, relief holes could be placed in the sides of the feedthrough tubes to reduce the trapping efficiency of the volume therein.

Absorption of gas by the scintillator has also been detected by measuring the output of the scintillator under various conditions. Figure 15 shows the decay in scintillator counting rate after evacuation of the counter. The relatively slow decrease is evidently due to the absorption of sample. Reducing the amount of absorption

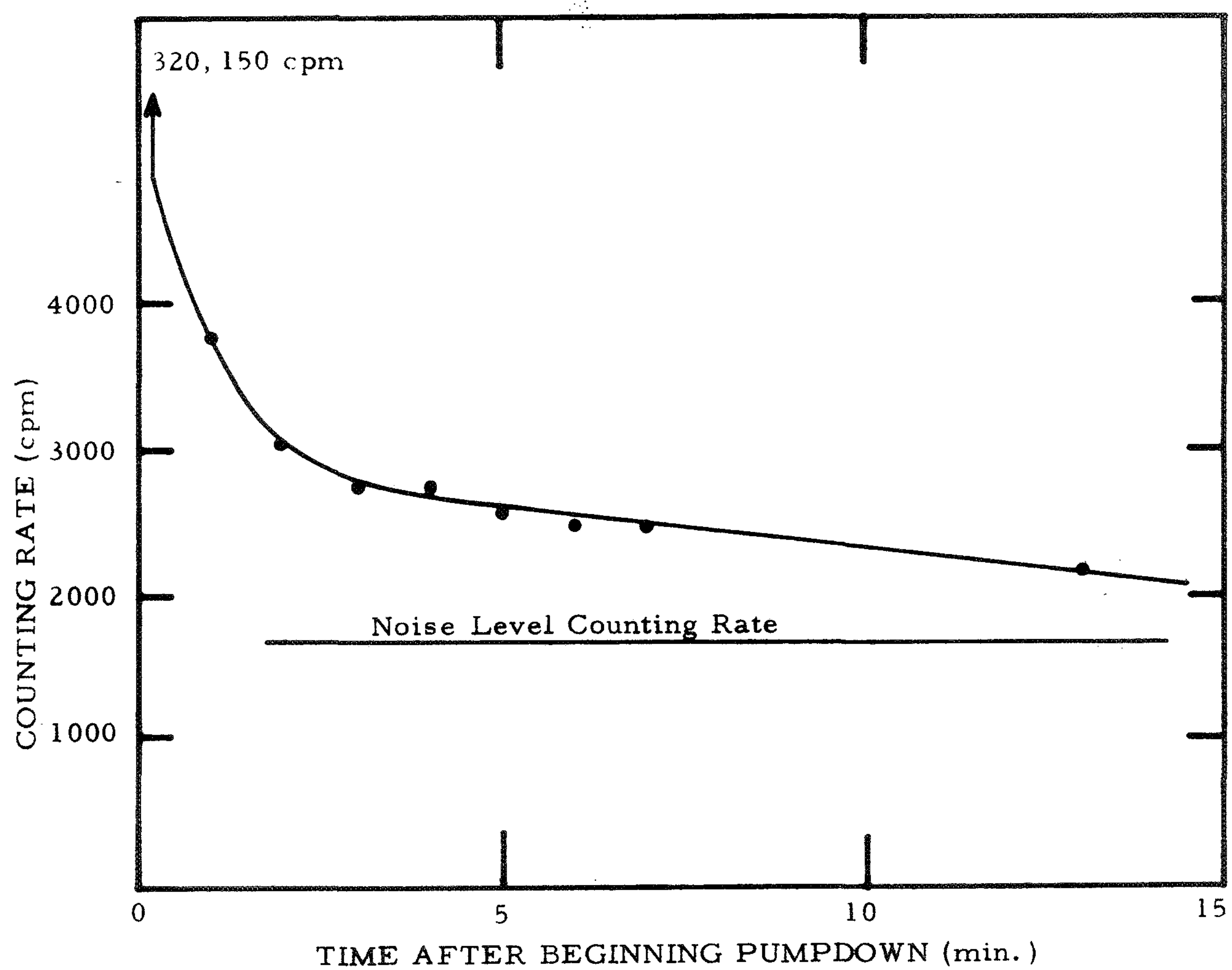


Fig. 15. Decrease in counting rate of the scintillator after soaking for 10 minutes with a sample producing 320, 150 cpm. Correcting for noise, the time constant for the decay is approximately 20 minutes after the first 3 minutes of counting.

can be accomplished by achieving a better coating of the scintillator material. The vacuum evaporated aluminum coatings used in the present work have been observed to have pin holes. Considerable effort was undertaken to reduce the number of these pin holes by removing as much dust from the surface of the scintillator as possible prior to the coating operation. This was accomplished by exposing the scintillator blocks to the beta rays from a very strong strontium-90 source to neutralize the electrostatic charges which grip the dust particles to the scintillator, and blowing a stream of dust-free gas over the surface just prior to insertion of the units into the vacuum system used for the metalization process. Nonetheless, some pin holes are still evident. A more satisfactory coating could have been applied if a glow discharge cleaning apparatus were available. As this equipment is not on hand at this time, the only method of cleaning the scintillator prior to evaporation has been with the radiation source. It is quite likely that with the proper equipment for cleaning and evaporation and/or sputtering of the metallic coating, a much more satisfactory sealing of the scintillator from the gas volume can be obtained. Even a coating as thick as 1 mil of aluminum will not seriously interfere with the anti-coincidence technique.

In the event that a cesium iodide scintillator is selected to replace the plastic scintillator, it is likely that the amount of absorption will be completely negligible, allowing full realization of the desired count rate reduction factor of $10^{-5}$. It should also be noted that the above data were taken using extremely hot sample and allowing the sample to equilibrate with the counter for a long period of time (nearly one hour) prior to the initiation of the experiment.

## 4.6 Detector Voltage

Plots of plateaus for operation in the proportional region are shown in Figures 16 and 17. On most of these plateaus the width is greater than 250 volts and the slope is less than 3% per 100 volts, indicating that the detector output would be relatively insensitive to fluctuations in the high voltage supply. Figure 16 demonstrates that the plateau characteristic is essentially independent of counting rate. Figure 17 demonstrates changes in plateau characteristics with gas pressure. Note that an applied potential of 1400 volts falls on all plateaus between pressures of 0.33 and 0.66 atmosphere.

## 4.7 Optimum Operating Conditions

The optimum conditions for operating the proportional counter depend upon a number of factors, including gas composition, presence or absence of electro-negative impurities such as water and oxygen, gas pressure, and the noise level of the electronic system used to read out the counter. Thus, it is not possible to specify a single set of operating parameters without detailed knowledge of these factors. However, a suggested set of operating conditions for counter #1 and counter #2 is given in Table IV for a gas composition of 90% argon - 10% $CO_2$.

## 4.8 Dead Volume

The critical volumes of the proportional counter system are given by region of interest in Table V. It is obvious that the quantity of gas in the gas flow tubes and in the cylindrical cavities at each end of the

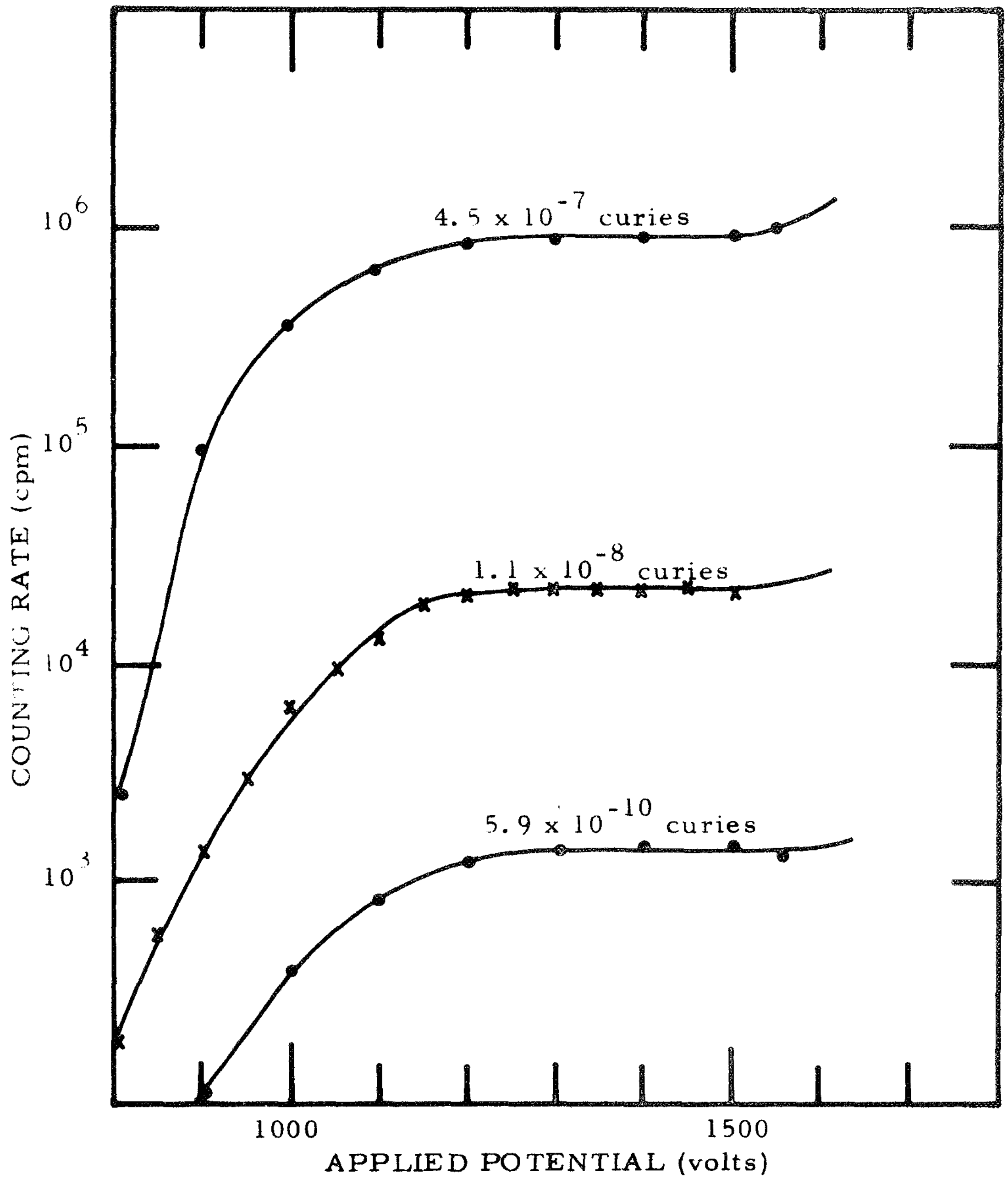


Fig. 16. Counting plateaus for low, medium, and high $^{14}CO_2$ sample activities. Counter #2 at 0.5 atmosphere, 90% Ar - 10% $CO_2$.

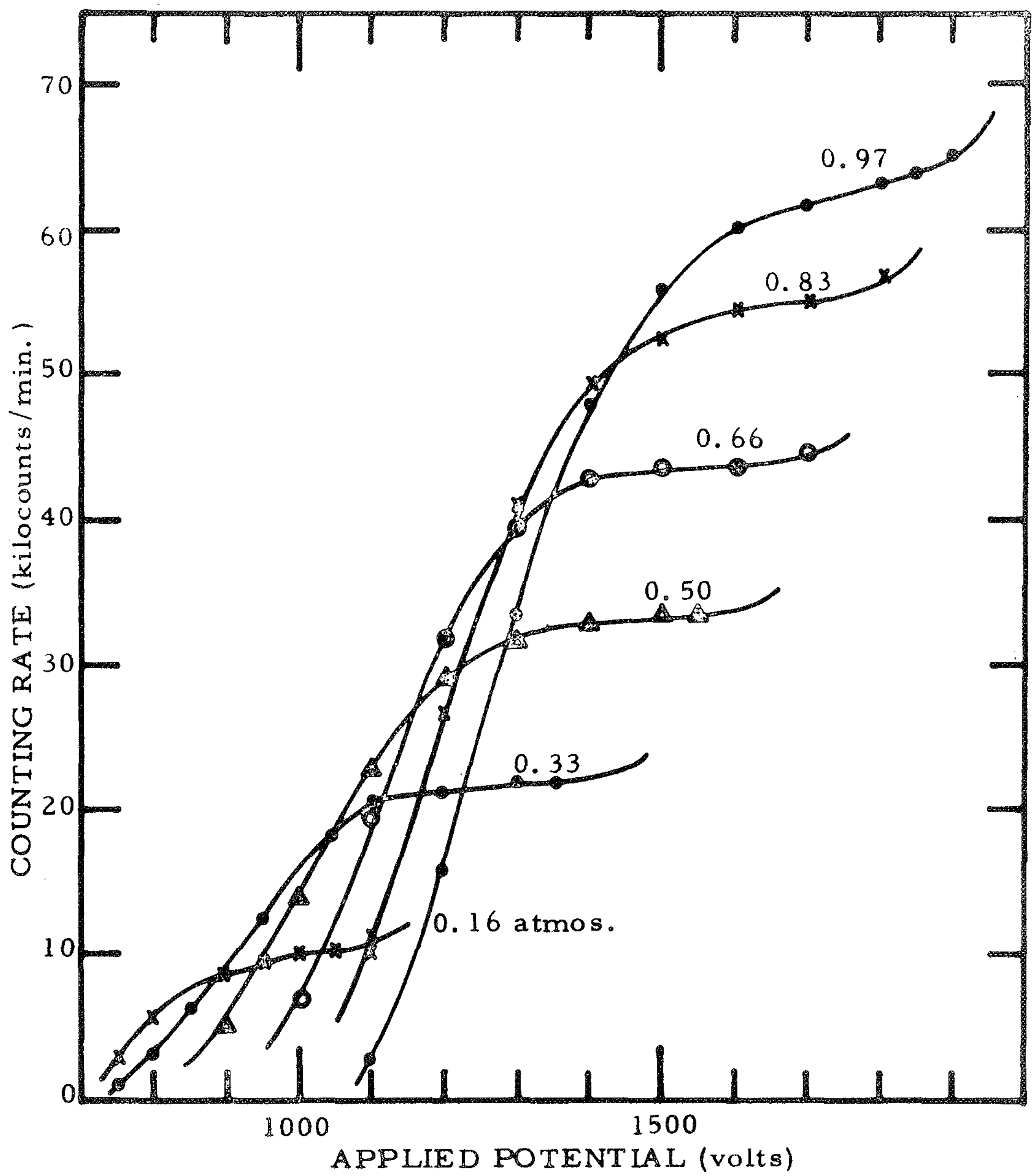


Fig. 17. Effect of gas pressure upon onset, length, and flatness of the plateau (proportional region) for counter #2 filled with 90% Ar - 10% $CO_2$ (including 32 nanocuries/atmosphere $^{14}CO_2$).

Table IV. Recommended Operating Conditions for the Two Carbon-14 Detection Systems

| | Detection System #1 | Detection System #2 |
|---|---|---|
| Proportional Counter Bias* | +1700 V. | +1400 V. |
| Photomultiplier High Voltage | +1500 V. | + 670 V. |

For both detection systems, the amplifier and discriminator requirements are:

| | |
|---|---|
| P. C. Overall Gain | 20 volts/picocoulomb (for a 30 pF capacitance due to counter and connecting cable, minimum signal is 0.3 millivolt; overall voltage gain required is 600) |
| P. C. Discriminator Setting | 0.2 volts |
| Scintillator Overall Gain | 1.3 volt/picocoulomb (for a 30 pF capacitance, minimum signal is 5 millivolts; overall voltage gain required is 39) |
| Scintillator Discriminator Setting | 0.2 volts |

* Assumes a gas composition of 90% Ar-10% $CO_2$.

Table V. Volumes of Critical Regions in the Proportional Counter

| Region | Volume in Region ($cm^3$) | Percent of Total Volume |
|---|---|---|
| Spherical halves (two) | 13.7 | 92.3% |
| Cylindrical section (one) | 13.9 | |
| Gas flow tubes (two each at 5" long, 0.107" I.D.) | 1.5 | 5.0% |
| Insulator cavities (two) | 0.8 | 2.7% |
| Total Volume | 29.9 | |

sphere (Fig. 2) are not in the sensitive region. This is true in the latter case because the large anode structure does not provide any appreciable gas gain so that any pulses produced in these two cylindrical cavities will be below the electronic noise level and hence undetectable. In addition, a small region exists near the point where the wire enters the insulated feedthrough bosses wherein the gas multiplication factor is lower than that along the major portion of the wire. In Figure 18 are presented data on this effect obtained by Benjamin in a counter of quite similar design. It is seen that the length from the bosses to where the gas gain reaches 30% or more of its final value is approximately 0.05 of the counter radius. Assuming such counts will not be properly registered, the additional dead volume due to this effect can be calculated from the fraction, f, of a spherical volume enclosed by a section located a distance a/r from the spherical surface by the formula

$$f = 1/2 \left(\frac{a}{r}\right)^2 \left[3 - \left(\frac{a}{r}\right)\right]$$

The result of this calculation shows that the spherical cavity itself is 99.6% effective. Thus, the only appreciable dead volumes in the system are those associated with the flow tubes and insulator cavities, which in the present design means that 92.3% of the counter volume is active. It is noteworthy that the gas-flow tubes are considerably larger in diameter than necessary so that by reducing their size, it would not be difficult to achieve an active volume in the counter of 95 to 96% of the total volume of the gas sample.

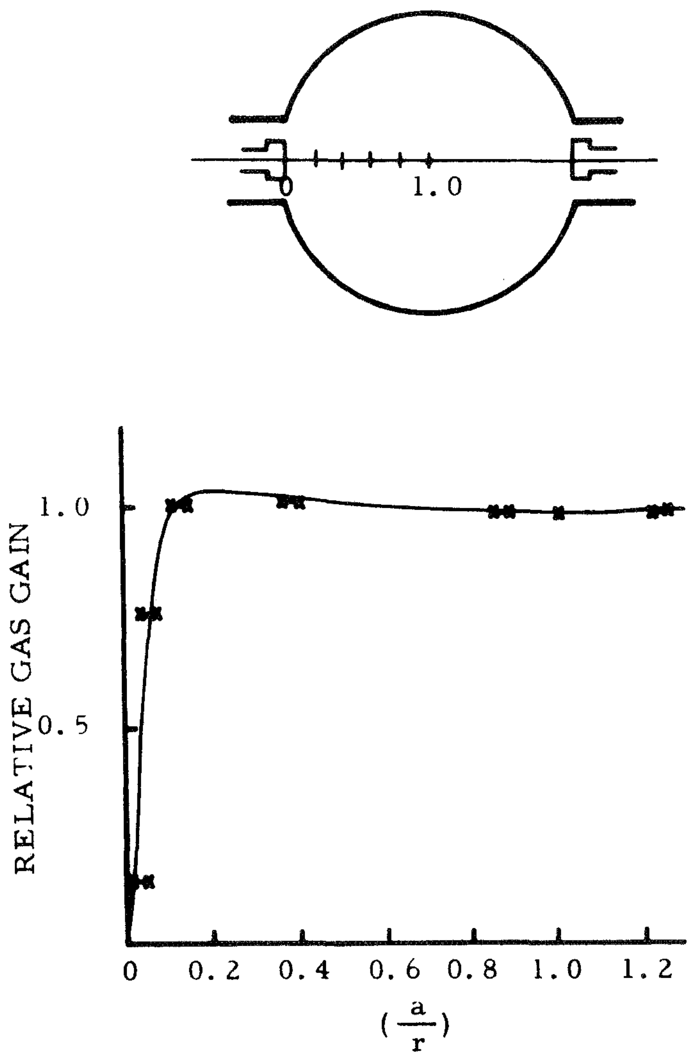


Fig. 18. Variation of pulse height along the axis of a spherical proportional counter built with the same relative dimensions as the carbon-14 counter. Taken from Benjamin, et. al. (Be-68).

## 4.9 Detection Efficiency and Calibration with $^{14}CO_2$

Although the active volume is high, the question arises as to the efficiency with which the counter can detect the carbon-14 beta emissions. Inspection of Figure 11 shows that over 95% of the beta rays are emitted with an energy in excess of a few keV. Thus, if the counter is capable of detecting energy depositions below a few keV, it will have an excellent efficiency for detection of the carbon-14 beta rays. This, in fact, has been achieved and is demonstrated clearly in Figure 10 and Figure 19. In this second figure one sees that below an energy discriminator level of about 1.5 keV, the counting rate changes very little all the way down to a level of approximately 0.3 keV, indicating virtually complete detection of the emitted radiation. Below this point the count rate rises because of interference from electronic noise associated with the input stages of the preamplifier.

Another check on detection efficiency is obtained by varying the gas pressure to see if any detectable fraction of the radioactivity is escaping to the walls. This comparison has been made by dividing the counting rate by the pressure at which the data were taken. These results are presented in Figure 20 where it is seen that the plateaus correspond within statistical error to the same sample activity, independent of pressure.

From these two observations we conclude that the proportional counter, when operated at a low level discriminator setting of 1 keV or less, has from 98 to 100% efficiency for detecting beta rays in the live volume of the counter. In addition, some of the

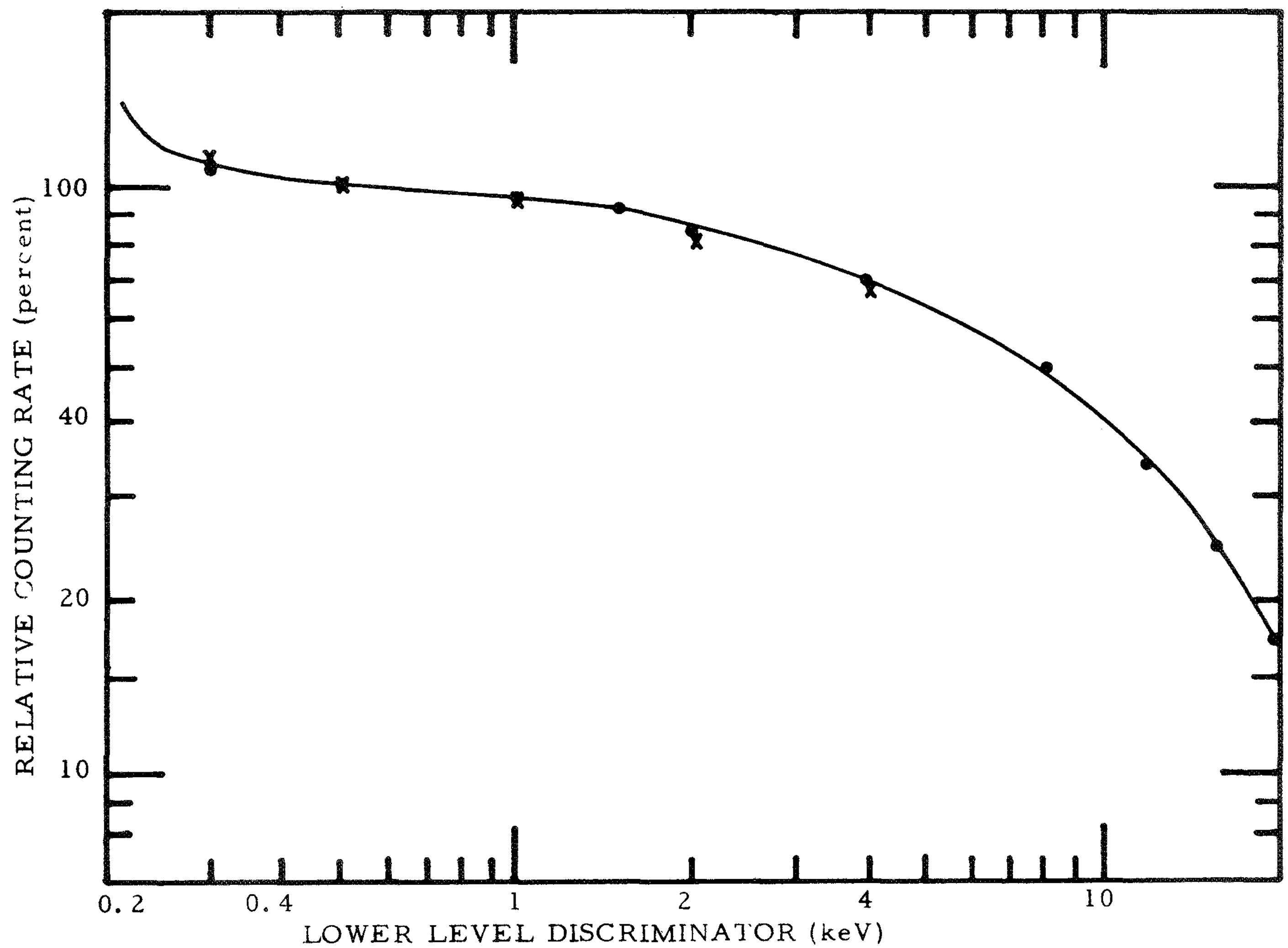


Fig. 19. Integral $^{14}C$ spectrum showing excellent flatness of the spectrum below 1 keV. Data taken with counter #1 filled to 0.5 atmosphere with P-10 gas and 18% of $CO_2$ (including one nanocurie of $^{14}CO_2$). Bias was 1500 V., producing a gas gain of 300. Noise is encountered below 0.2 keV.

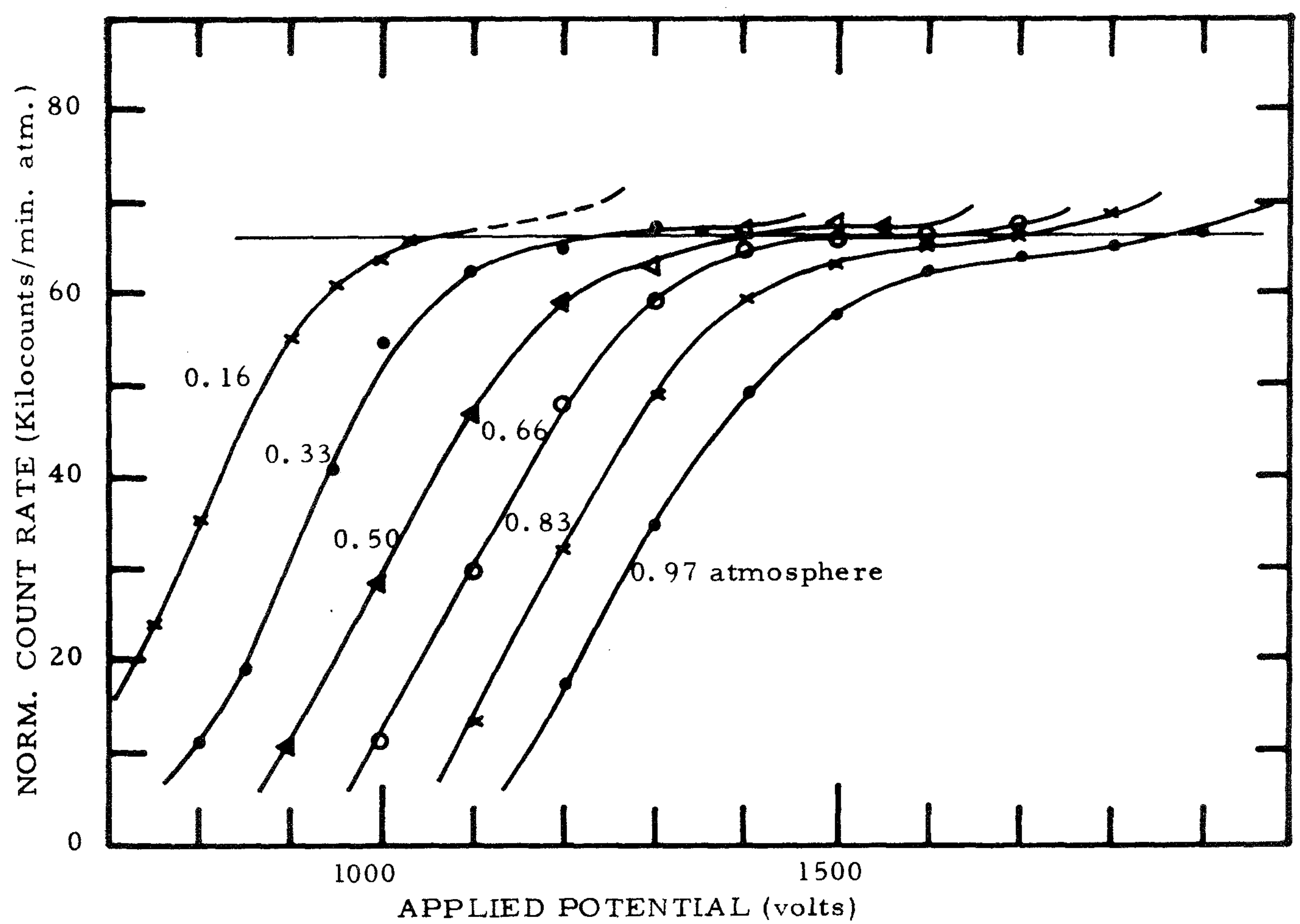


Fig. 20. Counting rate divided by gas filling pressure to show independence of determined activity upon operating pressure. Data is same as in Fig. 17.

beta rays emitted in the dead volume of the cylindrical cavities will pass into the main volume of the counter and be recorded. Thus, even these regions are, to a certain extent, active. The best estimate of detection efficiency for the system, including the losses due to dead volumes and a possible 1 or 2% loss in counting efficiency, provides an overall estimate for the present system of 92% efficiency for detecting carbon-14 radiation. Reduction in size of the gas flow tubes could raise this figure to 95%.

The calibration factor for the present system is therefore

$$4.90 \times 10^{-13} \text{ curies/cpm}$$

To obtain the activity of a measured sample in curies, this calibration factor is multiplied by the observed counting rate (in counts per minute).

## 4.10 Dynamic Range

The design goal sensitivity for detection of carbon-14 has been established to encompass the range 25 picocuries to 2.5 microcuries. Attainment of the lower limit of detection is contingent upon the background level and therefore upon the radiation sources to which the counter is exposed. The equations for calculating minimum detectable activities have been developed and are presented in Appendix A. For the conditions existing in the Radiation Instrumentation Laboratory at Avco/Tulsa the background counting rate under optimum anti-coincidence conditions is 7 cpm with an overall detection efficiency for carbon-14 of 72%, yielding a figure of merit (see Appendix A) of 27. Optimum conditions for an end-on exposure to the SNAP-19 source located one meter from the shielded counter were reached with a figure of merit of 6.2. Assuming it is required that the total count be more than 4.76 standard deviations above background (see Appendix A), and that the counting time is 30 minutes, the minimum detectable activities of carbon-14 are 1.4 picocuries for the laboratory environment and 7 picocuries for the SNAP-19 environment.

The upper limit of the targeted dynamic range is 2.5 microcuries, which will produce a counting rate of approximately 4,000,000 cpm under optimum conditions for rejecting background. This is easily realized with the present counter, provided high speed electronics are used to amplify the signal pulses. Since the rise time of the pulses is 1.5 microseconds, reliable counting rates could theoretically be achieved in the neighborhood of $10^7$ counts per minute. Using research quality nuclear electronic equipment, we have demonstrated counting rates as high as $10^6$ cpm in the laboratory with no evidence of counter malfunction. At high counting rates the pulse rise time and the time constants of the electronic circuitry determine the loss in counting efficiency due to near-coincident pulses. These losses can be tolerated, however, since one need only provide the necessary calibration curve to convert an indicated counting rate into a true counting rate. Such conversions can be accomplished with high accuracies.

### 4.11 Reproducibility

The reproducibility of the counter output for data taken sequentially has been studied to ascertain the level of precision. Hopefully, with careful design one should be able to achieve a reproducibility that is limited only by the statistics of particle emission and not by instrumental factors. In Table VI, data are presented of counts taken at high and low levels of carbon-14 to test whether the dispersion in counts follows the Poisson statistic. We have applied the Chi-square test to this data. The results obtained are that P = 0.3 for the two cases, where P is the probability that upon repeating these experiments the data would show greater deviations than observed here. Thus, it appears that the counter indeed produces an output whose minor fluctuations represent the randomness of the nuclear events and not erratic behavior of the instrument. It is to be noted that the relative standard deviations will be 0.1% and 1.6% for the two cases, thus demonstrating a very high level of precision.

### 4.12 Geiger Mode of Operation

Although the counter has been operated in the proportional region for most of the experiments presented in this report, some ancillary experiments were performed operating the counter in the Geiger mode. The method of operating the device as a Geiger counter is shown in the schematic diagram of Figure 7. Here the 10 K ohm resistor was varied until a pulse time comparable to that observed with the proportional counter was obtained. Higher values of resistor give pulses of greater width, thereby seriously affecting the high count rate capability of the detector. On the other hand, reducing the pulse time also significantly reduces the pulse output amplitude to the extent that with the 10 K resistor in place, it is necessary to use a preamplifier in order to satisfactorily detect the pulses. Thus, the one significant advantage of Geiger operation over proportional counter operation, namely, that the electronics

Table VI. Reproducibility at High and Low Counting Rates ($^{14}CO_2$)

| Measurement Number | Count in One Minute | Deviation from Average (%) |
|---|---|---|
| 1 | 934, 661 | +0.08 |
| 2 | 932, 624 | -0.13 |
| 3 | 932, 940 | -0.10 |
| 4 | 935, 178 | +0.14 |
| 5 | 933, 812 | -0.00 |
| Average | 933, 843 | P = 0.3 |
| | | |
| 1 | 3386 | +1.3 |
| 2 | 3325 | -0.5 |
| 3 | 3269 | -2.2 |
| 4 | 3379 | +1.1 |
| 5 | 3440 | +2.9 |
| 6 | 3257 | -2.5 |
| 7 | 3341 | -0.0 |
| Average | 3342 | P = 0.3 |

required is simpler, is largely negated by the desire to extend the upper counting-rate limit of the device. In addition, although the pulses were successfully shortened, a recovery time of the order of tens of microseconds was observed between the generation of a pulse and the time required for succeeding pulses to attain the original constant pulse height typical of the Geiger region.

In Figure 21 a plot of the plateau observed for the counter in the Geiger mode is shown compared to a plot of the plateau of the counter with the same gas sample, but operated as a proportional counter. It is obvious that the Geiger plateau is very poor and nearly undefined. This is largely due to the fact that the gas is an argon-$CO_2$ mixture containing no hydrocarbons. As mentioned in our original proposal, $CO_2$ is not a suitable quench gas for Geiger operation, although it is quite satisfactory for use as a quenching agent in a proportional counter.

Thus, for the following three reasons, proportional counting is to be recommended in lieu of Geiger counting:

1. Rapid pulse counting is possible in the Geiger mode only at the sacrifice of signal level.

2. Stable operation of the counter (wide plateau) is possible only if a hydrocarbon quench gas or other suitable quenching agent is added to the carrier gas.

3. In the Geiger region no pulse height discrimination is possible, thus eliminating the ability of the counter to

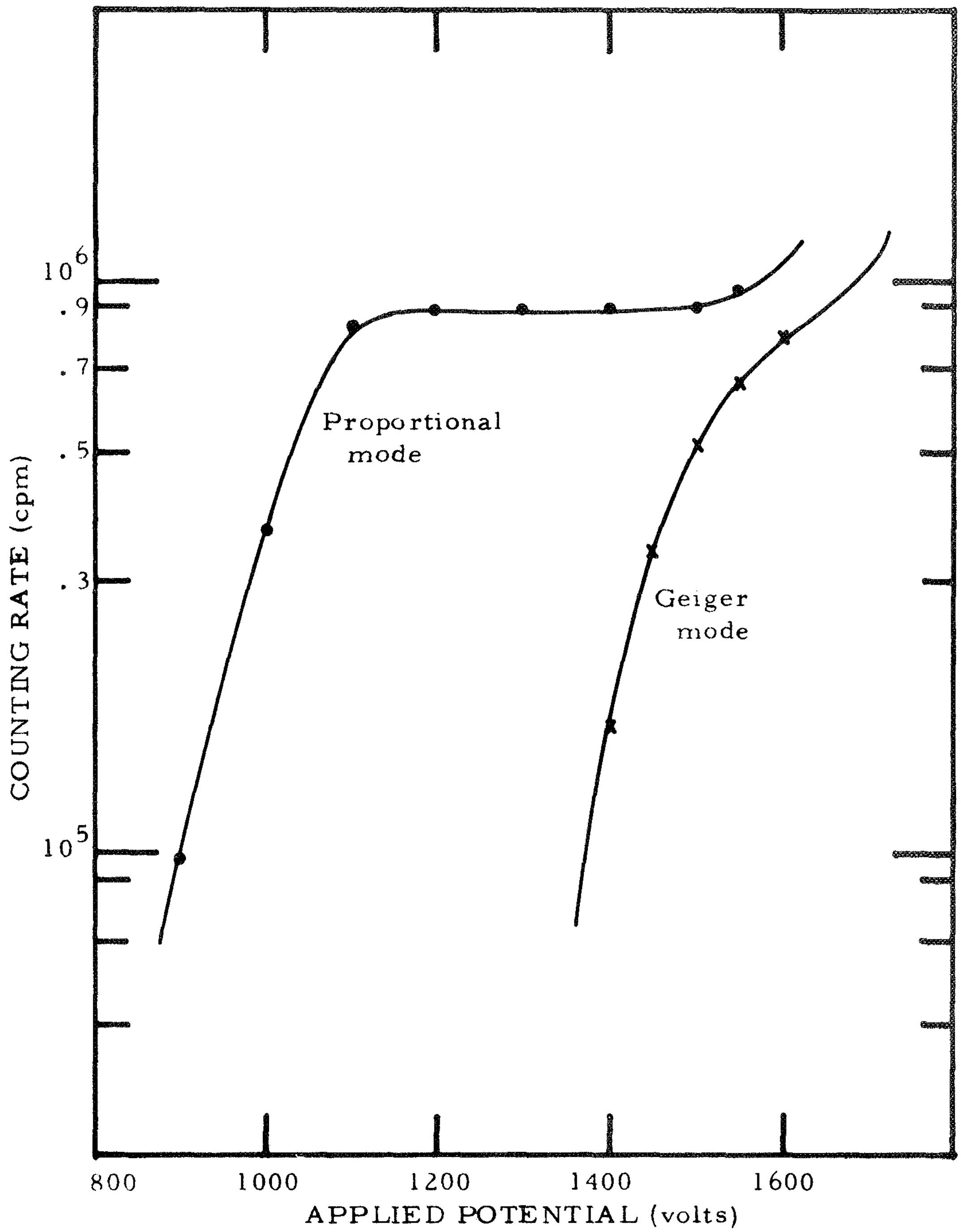


Fig. 21. Comparison of proportional and Geiger plateaus for counter #2 filled at 0.5 atmosphere with 90% Ar, 10% $CO_2$ (including 0.45 microcuries $^{14}CO_2$).

distinguish between heavy charged particles (e. g., cosmic rays or neutron recoils) and beta or gamma rays.

Finally, since the electronics required for a charge sensitive preamplifier can be had for only a very slight increase in weight and power over the amount of electronics that will be required for the total instrument, the proportional counter mode appears to clearly be the preferred mode of operation.

## 5.0 RADIATION INTERFERENCE

### 5.1 General

In addition to the natural radiation background from the Martian terrain, galactic cosmic rays, and solar flare radiation, there will be large amounts of the radioisotope $^{238}Pu$ on board the lander to provide thermal and electrical power. The latter device (RTG) will be a very strong source of gamma rays and energetic neutrons.

The natural environment includes the solar flare charged particle events. The flux of protons of energy greater than 55 MeV can be as high as $10^7$ protons/cm$^2$ per event and about 100 times this amount per year. These integrated fluxes are not of a sufficient level to cause radiation damage to the detection system. However, at the time of peak intensity during a solar flare particle event, the high flux of radiation could potentially cause severe interference with the life detection experiments. Peak intensities of past solar events at a position in space near the Earth are 8000 protons/cm$^2$ sec above 30 MeV (We-64).

As the projected flight date for Project Viking is 1973, solar flare activity should be very near its minimum, corresponding to the solar cycle sun spot minimum expected in 1974. Of course, flare-induced particle events occur also during solar minimum, but at lower frequency and generally at lower intensity.

The galactic cosmic radiation dose rate beneath the 5 g/cm$^2$ atmosphere on Mars is expected to be less than 30 mr/day at flare minimum. This corresponds to a charged particle flux rate of from one to ten particles/$cm^2$ sec. The radiation from the planetary $^{238}U$, $^{232}Th$, and $^{40}K$ is expected to be less than 1.0 mr/day. This background is completely negligible in comparison with cosmic rays and the background radiation produced by the on-board RTG.

The $^{14}C$ radiation detection system has considerable capability toward minimum possible response to the above extraneous radiation sources. All charged particles which enter the proportional counter from the outside must first traverse at least 0.25 inch of scintillator shield and will deposit no less than 1 MeV of energy. This can be readily detected by the photomultiplier tube. The scintillator has been designed to completely surround the counter volume, and the gas flow tubes have been positioned so that they do not provide "holes" through which external radiation can reach the counter without passing through the scintillator. Thus, rejection of unwanted counts from external charged particle radiation should be extremely efficient, provided the electronics can handle the extremely high counting rates (up to 80 kHz) for the solar flare radiation. Galactic cosmic rays will be very simple to discriminate against because of their low flux and ease of detectability.

## 5.2 Radiation Interference from the RTG

The carbon-14 detection system is designed to provide both bulk shielding against external radiation and rejection of unwanted pulses in the counter by operating it in anti-coincidence with the scintillator shield. The shielding strongly attenuates the low energy protons and low energy gamma rays which impinge upon the detector. However, it is impractical to try to provide all the attenuation necessary to reduce either the charged particle background or the gamma ray background to acceptable limits.

The anti-coincidence shield should be fully effective in rejecting all external charged particle background radiation. However, such a shield cannot reject the RTG gamma ray background except for those gamma rays which interact with the scintillator material. Fortunately, this does provide an excellent basis for discrimination, although it cannot be 100% effective. The discrimination is possible, per the following rationale: A proportional counter generally has a counting efficiency for gamma rays of 1%/MeV per gamma ray. A simple calculation shows that the probability of a gamma ray interaction with the gas of the counter is nearly a factor of 100 below this. This means that most of the counts recorded are due to electrons rejected from the counter wall by the gamma rays. Thus, if the counter wall were a separate detector which could be operated in anti-coincidence with the gas volume, the response to gamma rays would be much less. On the other hand, $^{14}C$ beta particles emitted by the gas and entering the wall also could be rejected by anti-coincidence. Thus, optimum operating conditions have to be selected experimentally.

To measure the background interference due to the RTG's, experiments have been performed with a SNAP-19 capsule of the type used to fuel the RTG's. This work was done at Mound Laboratory, Miamisburg, Ohio, operated for the AEC by Monsanto Research Corporation.*, The experiments were performed in Building 45 at Mound Laboratory which is especially constructed with a high ceiling and false floors over a pit to minimize radiation scattering.

---

* We would like to especially thank Mr. B. D. Scearce, Mr. Ed Anderson, and Mr. Dick Neff for their assistance in connection with these experiments.

The SNAP-19 unit was placed on a thin vertical rod approximately five feet above the floor. This rod could be rotated by a servomotor to position the SNAP unit at any orientation with respect to the detection system (see Figure 22). The carbon-14 detection system was mounted above the gas flow system table so as to be at the same height as the SNAP unit. The preamplifiers were located on the gas flow table, but the electronic equipment for analysis of the pulses was located a few feet away behind paraffin blocks to minimize the dose to the person operating the equipment. Technical data on the SNAP unit employed in these experiments is given in Table VII.

### 5.2.1 General Features

The spectrum produced in the proportional counter by the SNAP-19 unit was measured and is presented in Figure 10. It can be observed here that if one places a threshold discriminator level at the higher energies, some discrimination is possible against the SNAP-19 radiation, compared to the carbon-14 radiation. However, as will be shown below, the figure of merit for the system is not significantly improved by raising the discriminator setting. In most of the data presented below, the proportional counter discriminator setting was 1 keV or less. The result obtained when the detection system was exposed to the SNAP in its broadside orientation at a distance of one meter and with no added shielding was the following:

Scintillator counting rate - 2,000,000 cpm

Proportional counter counting rate (no anti-coincidence) - 20,000 cpm

Anti-coincidence output - 2000 cpm

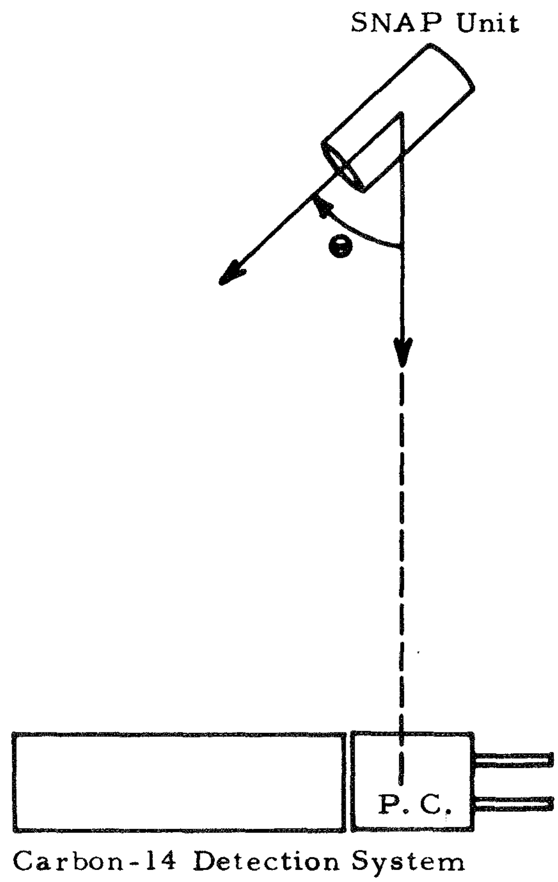


Fig. 22. Diagram showing the orientation of the SNAP-19 cylinder in terms of the angle θ. When this angle is $0^{o}$, the orientation is termed "end-on"; when $90^{o}$, it is termed "broadside".

Table VII. Description of the SNAP-19 Fuel Capsule Used in the Tests at Mound Laboratory*

Fabrication date: November 11, 1966

Fuel: Stoichiometric $PuO_2$

Wattage: 550.27 $\pm$ 1% Watts (thermal) (95% conf.)

Impurity Analysis (wt. % as plutonium metal) (dated 10/21/66):

| | |
|---|---|
| Nickel | 0.062% |
| Aluminum | 0.176 |
| Calcium | 0.095 |
| Manganese | -- |
| Silicon | Tr |
| Chromium | 0.074 |
| Copper | Tr |
| Zinc | 0.062 |
| Sodium | Tr |
| Iron | 0.340 |

Mass Spec. Isotopic Analysis (10/17/66):

| | |
|---|---|
| Mass 238 | 79.67% |
| 239 | 15.78 |
| 240 | 3.279 |
| 241 | 1.113 |
| 242 | 0.155 |
| 236 | $<$2 ppm |

Average Apparent Density of Fuel: 8.94

Crush Strength: 1100 (min), 1205 (avg), 1375 grams (max)

* These data were kindly furnished by Mr. B. D. Scearce of Monsanto Research Corporation.

Thus, the SNAP unit provides an extremely high background radiation which can seriously interfere with the proper operation of the carbon-14 detection system. In the experiments which follow we will demonstrate the method of approach in determining the optimum conditions for reducing this background counting rate in such a way that the detection of carbon-14 radiation is not compromised.

### 5.2.2 Effect of Distance

The variation of radiation count rate as a function of distance was investigated for two orientations of the SNAP unit with the detection system operated in the anti-coincidence mode. The results are shown in Figure 23. Although it might be expected that the observed counting rate would follow an inverse square law with distance, the exponent of the counting rate vs. inverse distance curve was found to be 2.15 for the end-on orientation and 2.55 for the broadside orientation. This departure from the expected exponent of 2.0 is evidently related to the fact (discussed below) that the anti-coincidence output is strongly dependent upon the energy spectrum of the radiation. Thus, it is likely that contributions of scattering effects to intensity and variations in spectrum are responsible for the non-ideal behavior.

### 5.2.3 Effect of the Orientation of the SNAP Unit

The output of the radiation detection system with the SNAP at a distance of one meter has been measured as a function of the orientation of the SNAP unit. Both the direct output of the proportional counter and the output of the anti-coincidence circuit were recorded. These counting rates were normalized to 1.0 with respect to the rate at an orientation of $90^{o}$. The results are presented in Figure 24. Here it

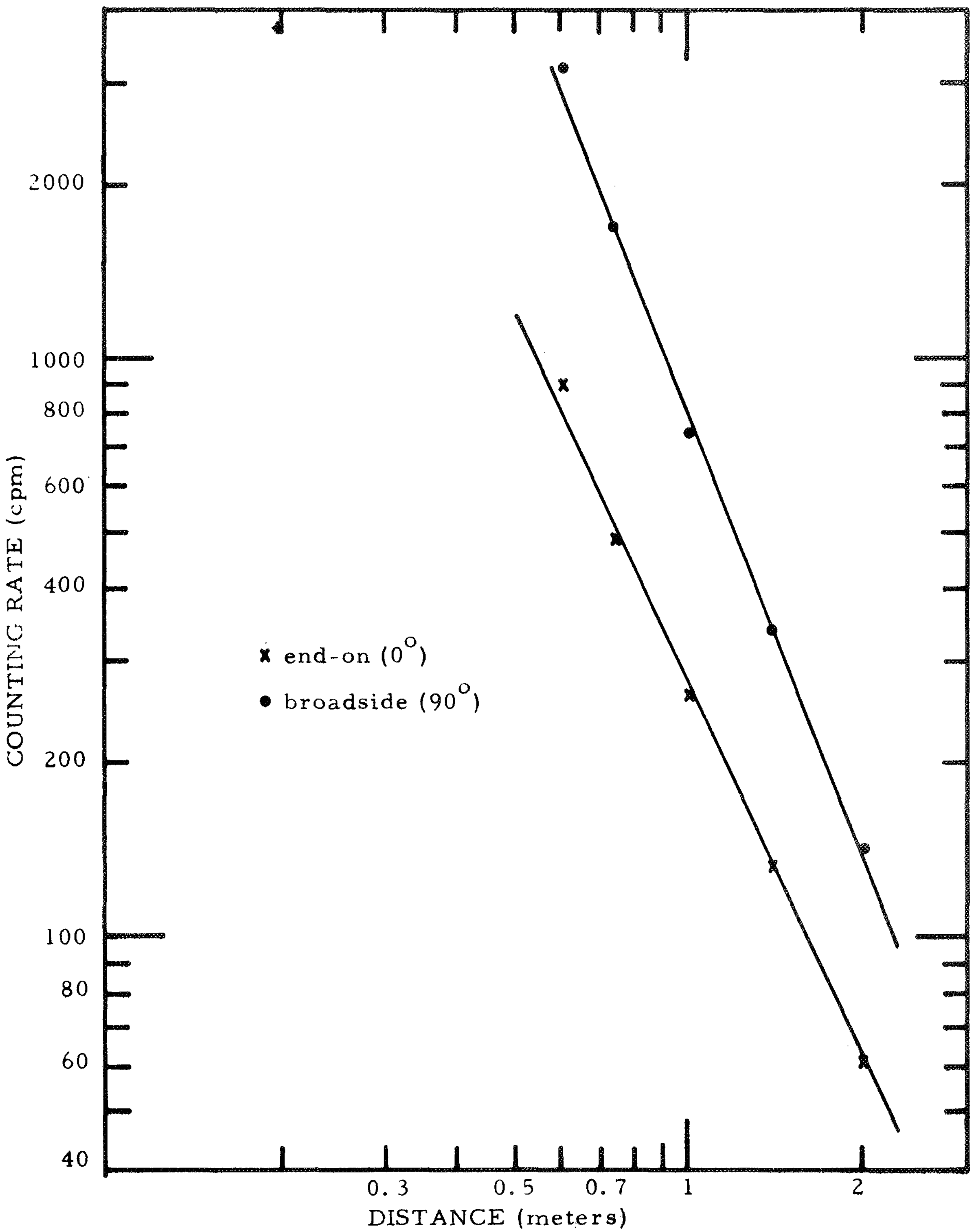


Fig. 23. Effect of separation distance between SNAP unit (at two orientations) and detection system. Counter #1 operated in anticoincidence mode. Includes 0.125 inches of tungsten shielding.

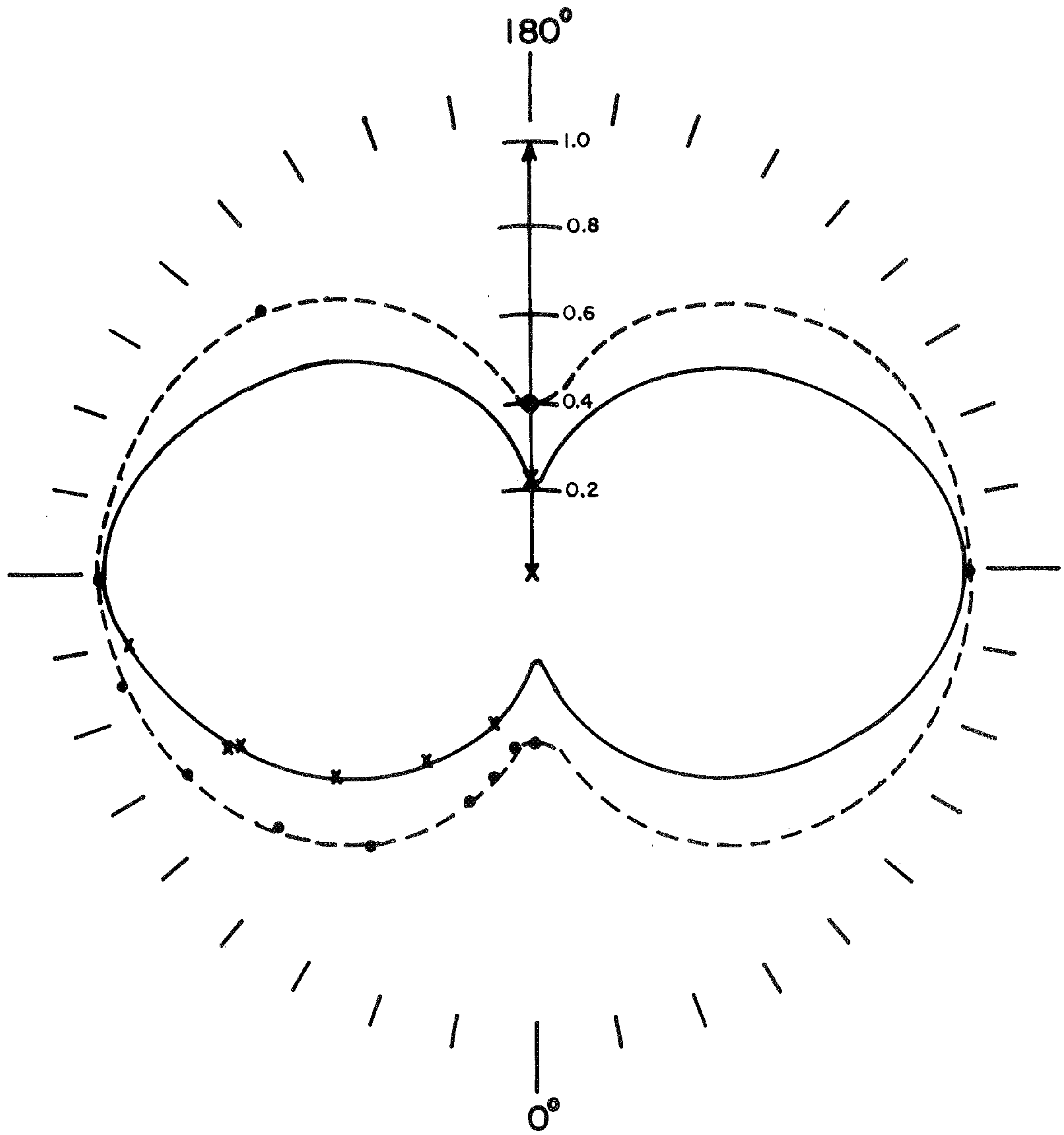


Fig. 24. Angular dependence of the radiation intensity emitted by the SNAP-19. Solid line is the anticoincidence output counting rate; dashed line is direct rate from proportional counter. Both rates have been normalized to 1.0 at an angle of 90°.

is seen that the SNAP-19 capsule emits a significantly greater radiation intensity from the sides (broadside orientation) than along the axis (end-on orientation). This is evidently because the encapsulating shell is relatively thin, providing very little attenuation of the significant radiation components so that self-shielding by the plutonium fuel is the important factor. Thus, some of the radiation emitted at one end of the capsule is absorbed before emerging from the opposite end of the capsule, whereas such effects are less important across the diameter which is roughly one-third the capsule length. When the proportional counter output is measured alone, the radiation intensity decreases to a minimum of 40% of the maximum level, whereas the anti-coincidence output reaches a minimum of 20%. Thus the orientation of the capsule is important not only for reducing gross counting rate, but even more important for reducing the rate when the anti-coincidence technique is employed. This can be explained on the basis of the higher background rejection efficiency for harder radiation (see Figure 29 below). This is indirect evidence that the radiation spectrum emitted from the end of the SNAP cylinder is indeed harder than that emitted from the sides, as would be expected from the source absorption effects considered above.

### 5.2.4 Effect of Shielding

In Figure 25 are presented data showing the reduction in counting rate achieved by adding tungsten* shielding between the detection system and the SNAP unit. It is seen that a relatively small amount of tungsten provides an initial big improvement in reducing background,

---

* Tungsten alloy containing 90% W, 6% Ni, and 4% Cu. Alloy number 1000, manufactured by Mallory Metallurgical Co., Indianapolis, Ind.

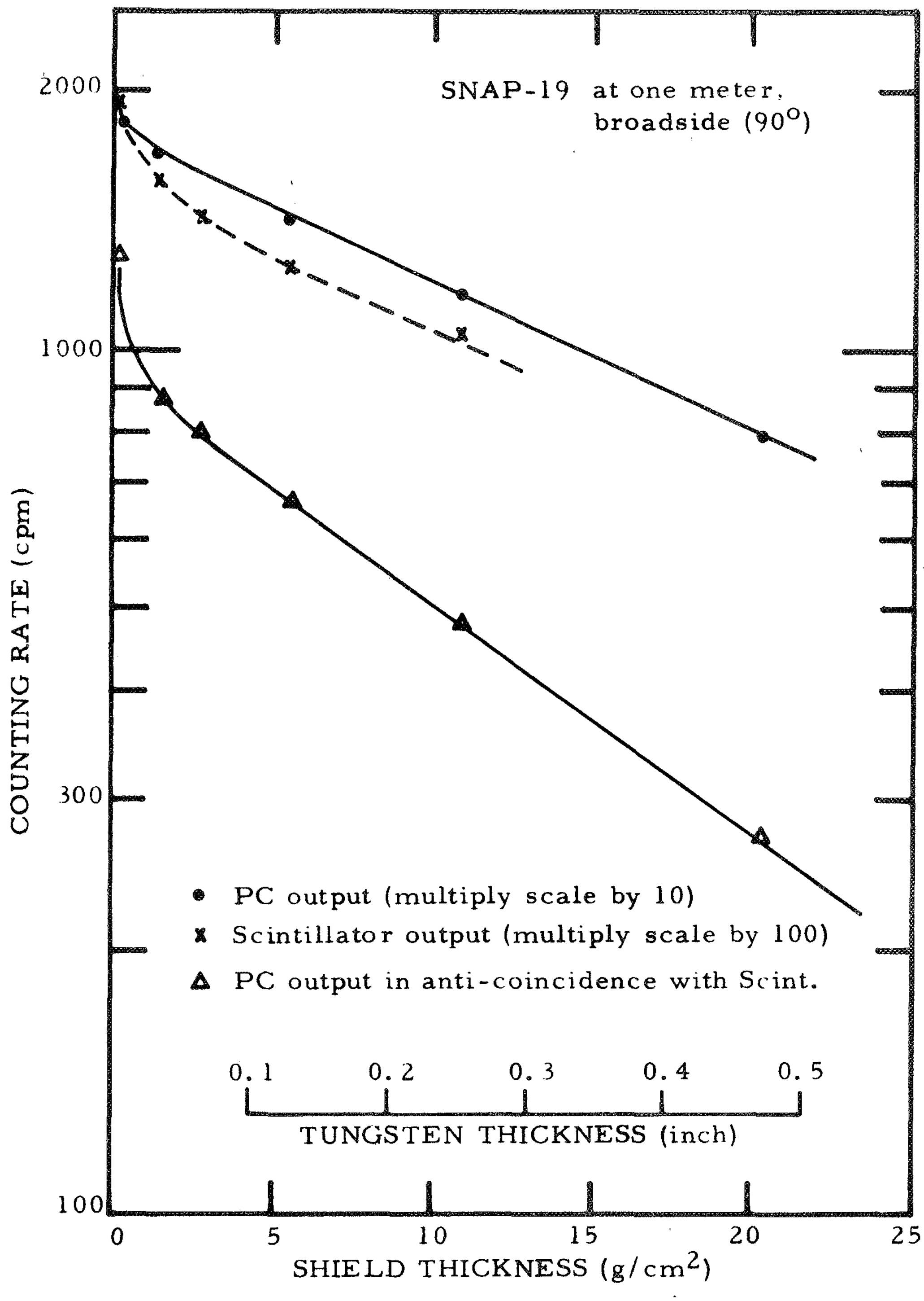


Fig. 25. Shielding effectiveness of tungsten (Mallory alloy 1000) in reducing counting rates for the scintillator, proportional counter, and anti-coincidence output.

but that subsequent shielding is less effective. Presumably there is a low energy component easily absorbed by the first 1/32" of tungsten. Also of note from this graph is that the slopes of the attenuation curves are different for the straight proportional counter output and the anti-coincidence output. This again is evidently because higher energy radiation is more effectively rejected by the anti-coincidence mode. The slopes of the two outputs for large shield thicknesses are 0.044 and 0.067 $cm^2/g$ for the straight and anti-coincidence outputs, respectively. These correspond to average gamma ray energies of about 2.0 and 1.0 MeV, respectively (Gr-57). These energies are well in the range of the known high energy gamma radiation emitted by plutonium-fueled SNAP units. Data obtained by others (Bl-68) have revealed strong gamma components at energies of 0.76 and 2.62 MeV. An effort was made to distinguish whether these components were indeed the main contribution to the observed counting rate or whether the neutron component of the SNAP emission was the important factor. It was observed that a polyethylene shield attenuated the background counting rate to an amount near that observed with tungsten when the two shield thicknesses were equivalent in mass thickness ($grams/cm^2$). This is in agreement with the interpretation of high energy gamma rays since the Compton scattering process is the dominant one at these energies. An additional factor rules out the likelihood of significant neutron counts. This is the energy spectrum produced in the proportional counter as recorded on a pulse height analyzer. The recorded spectra were nearly indistinguishable from those produced by high energy gamma sources and showed no evidence of pulses greater than about 50 keV, which would be produced by neutron recoil products. In addition, a theoretical analysis of the known neutron flux emitted by the SNAP unit predicts a counting rate considerably less than the counting rate produced by the known gamma emissions. Finally, experiments by Kaminskas, et al (Ka-69) with various detectors exposed to a SNAP-27 unit have shown that the background measured is almost wholly due to the gamma ray field, with an insignificant contribution from the neutron field.

### 5.2.5 Combined Effect of Shielding and Orientation of the SNAP Unit

In Figure 26 are shown the shielding curves for the anti-coincidence output for three orientations of the SNAP-19 unit. The data for each curve were normalized to the counting rate obtained at zero shield thickness. It can be seen that shielding effectiveness is much greater for the broadside orientation than the end-on orientation, again presumably due to the fact that the anti-coincidence output is strongly dependent upon the hardness of the radiation.

### 5.2.6 Summary of Results on Anti-Coincidence Effectiveness Factor, $M_A$

The anti-coincidence effectiveness factor, $M_A$, is defined as the proportional counter counting rate (no anti-coincidence) divided by the anti-coincidence output counting rate. The effect on this parameter of shielding thickness, orientation of the SNAP-19 unit, orientation of the detection system with respect to a fixed SNAP unit, and variations in energy spectrum of the radiation source have been determined. Results for the first two cases are shown in Figures 27 and 28.

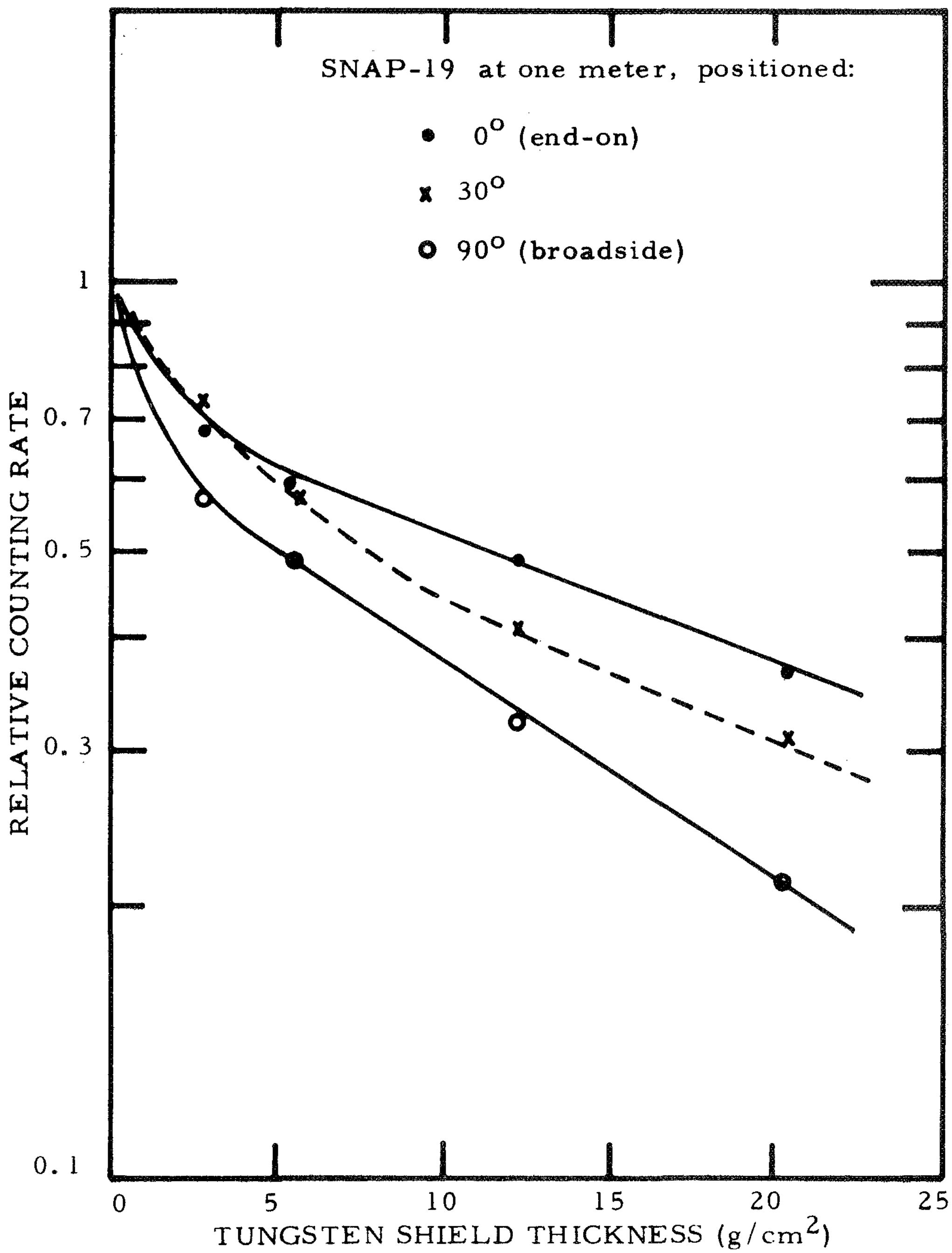


Fig. 26. Combined effectiveness of tungsten shielding and orientation of the SNAP unit.

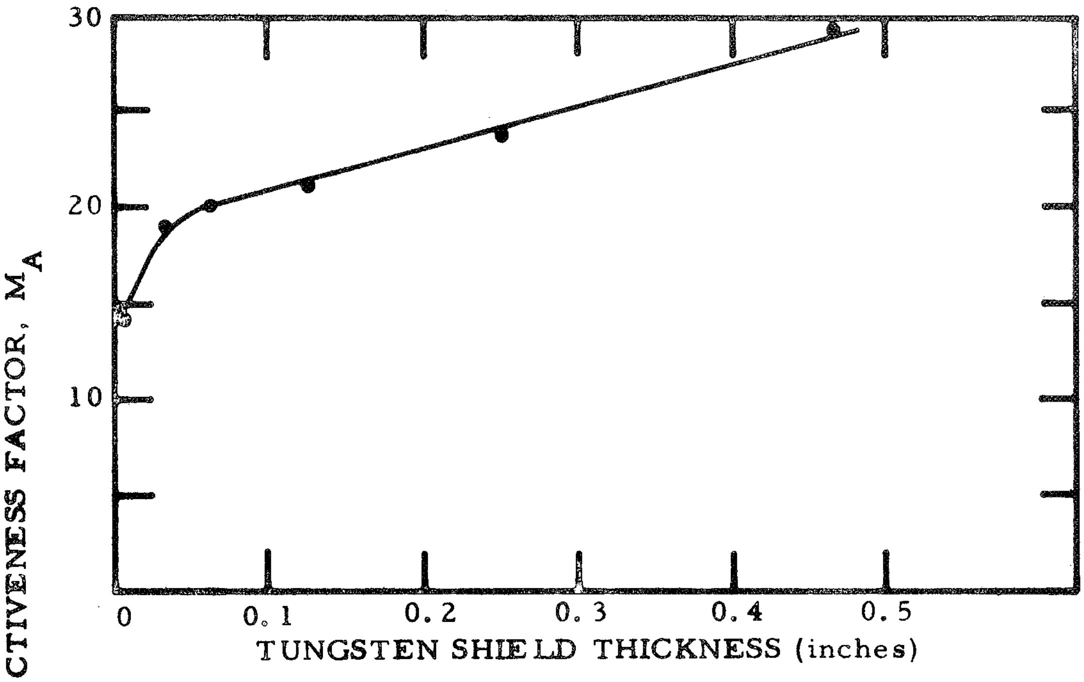


Fig. 27. Effect of shielding upon $M_A$. SNAP broadside.

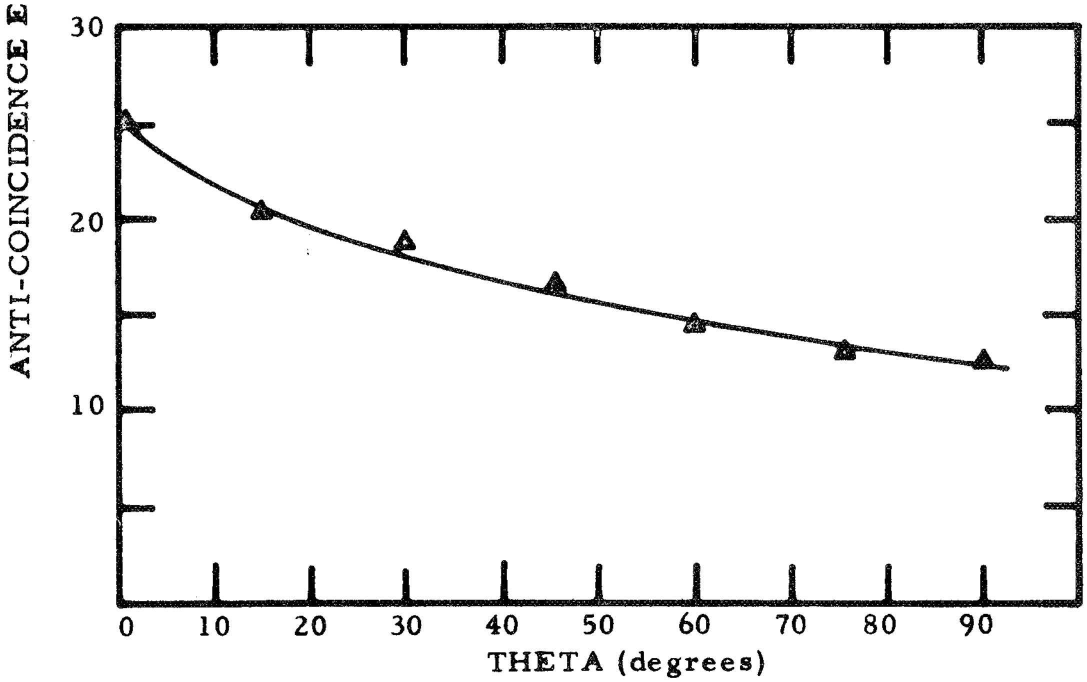


Fig. 28. Effect of orientation of the SNAP-19 source upon $M_A$.

In Table VIII are given the values of $M_A$ for four different orientations of the carbon-14 detection system with respect to the SNAP-19 system (in two cases, end-on and broadside). It is seen that there is only a small variation in shielding effectiveness factor with the orientation of the detection system and that the effectiveness is approximately 25 whenever the SNAP-19 is viewed along its axis and approximately 15 when viewed broadside. Thus, the carbon-14 detection system has an outstanding capability for rejecting radiation interference regardless of the direction of the external source. As discussed earlier, the counter was carefully designed so that the scintillator completely surrounds the proportional counter cavity and so that losses of anti-coincidence efficiency due to particles passing down the gas flow tubes are eliminated by judicious placement of the tubes.

In Figure 29, the anti-coincidence effectiveness is plotted for several radiation sources. It is seen that the rejection of the high energy gamma rays from the thorium-228 source is extremely efficient, reaching a factor of over 60. Maximum observed effectiveness factors for the SNAP-19 source were approximately 30, whereas for radiation sources of lower average energy such as cesium-137 (0.66 MeV) and the bremsstrahlung from the beta rays of strontium-90, the factors are much lower, in the neighborhood of 10 to 15.

Table VIII. Values of Anti-coincidence Background-Rejection Factor, $M_A$, (no shields, SNAP-19 at one meter) for Various Orientations of the Carbon-14 Detection System

| Carbon-14 Detection System | SNAP-19 | |
|---|---|---|
| Source toward: | End-on ($0^{\circ}$) | Broadside ($90^{\circ}$) |
| Photomultiplier end | 24.9 | 19.4 |
| Proportional counter end | 24.6 | 14.1 |
| Side, gas-flow tubes vertical | 21.4 | 13.2 |
| Side, gas-flow tubes horizontal | 25.4 | 12.7 |

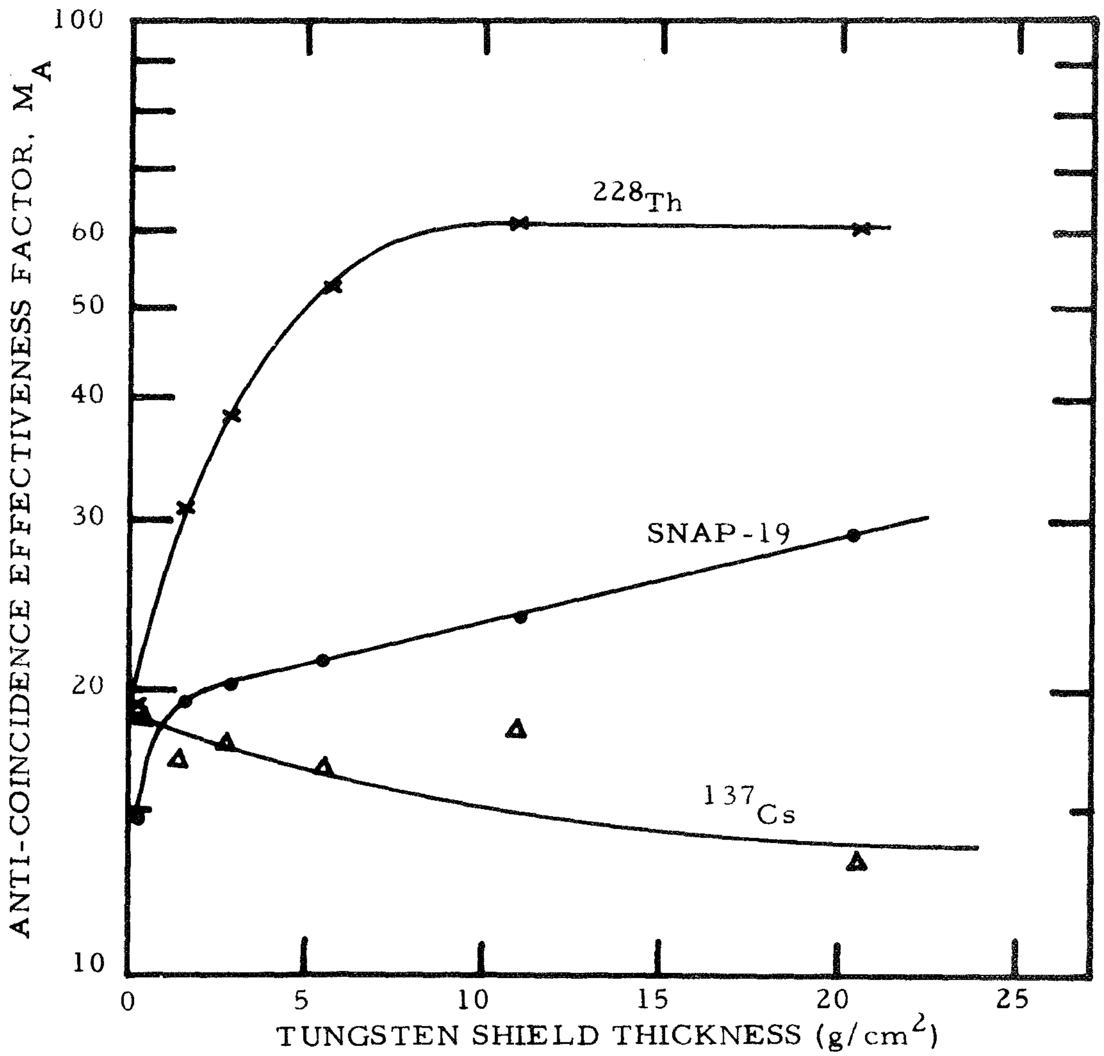


Fig. 29. Anti-coincidence effectiveness factor as a function of shielding thickness for three radiation sources. Changes in effectiveness are due to the effect of the tungsten shielding upon the energy spectrum of each source.

### 5.2.7 Effect of Varying the Gain of the Scintillator Output Channel

The efficiency of background rejection, as well as the efficiency of rejecting carbon-14 counts, can be varied by adjusting the voltage gain and/or low level discriminator in the scintillator channel. It is necessary to perform this adjustment in order to optimize the instrument for detecting the carbon-14 radiation in the presence of a high background level. It is noteworthy that for the maximum effectiveness of rejecting background, the gain must be set so high that a large number of noise pulses are produced by the scintillator. This is because the amount of energy deposition produced by the interfering gamma rays from the SNAP-19 is so low (as low as tens of keV) that the signal observed by the photomultiplier tube is often comparable with the tube's inherent noise level. One reason for this is that the quantum efficiency of the plastic scintillator and the rather long path length which the photons must traverse through the scintillator limit the amount of signal available to the photomultiplier. This situation could be improved somewhat by replacing the plastic with a cesium iodide scintillator and reducing the size of the scintillator and proportional counter. Although some noise pulses are produced by the scintillator output, experiments were performed to demonstrate that this did not provide false rejection of either background or carbon-14 counts through chance coincidence between radiation pulses and noise pulses.

In Figure 30 the efficiency for passing carbon-14 counts through the anti-coincidence circuit is plotted as a function of scintillator gain. Large changes in gain affect only slightly the number of carbon-14 counts rejected. This is chiefly because a large fraction of the

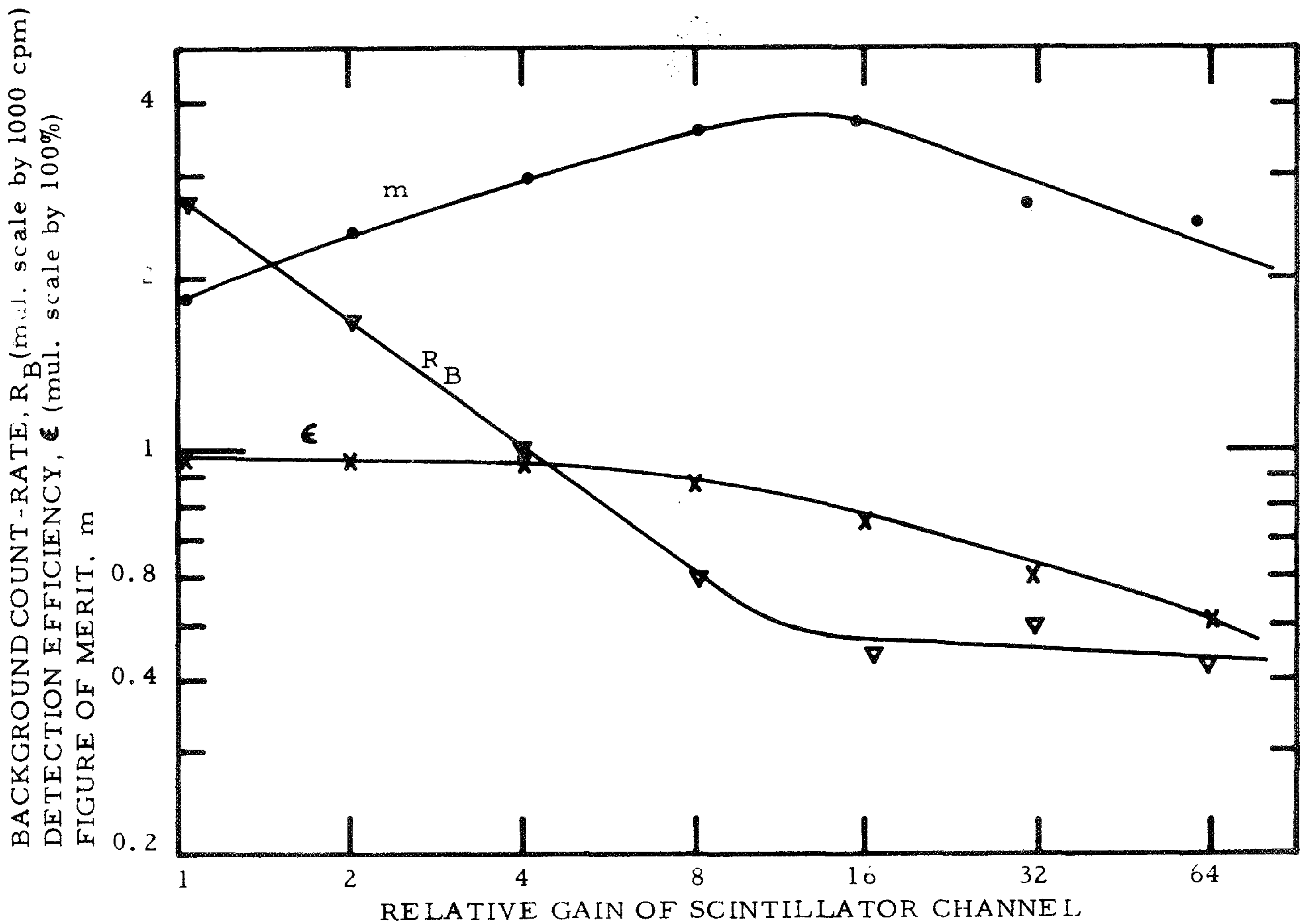


Fig. 30. **Effect of scintillator channel gain setting upon $\epsilon$, $R_B$, and m, showing method of determining optimum setting. SNAP-19 at $0^{o}$ (end-on), with detector shielded by 0.125 inch tungsten alloy.**

carbon-14 beta rays are either completely absorbed in the gas volume or deposit only a small, undetectable amount of energy in the scintillator. On the other hand, the rejection of background counts is strongly affected by such gain changes. The question naturally arises as to which gain setting is optimum for the problem at hand since higher gain provides better rejection of background, but at the same time less efficiency for counting the carbon-14. This problem has been analyzed mathematically in Appendix A. It is shown that for detection of the lowest possible level of source radiation superimposed on a constant background level, one must maximize the figure of merit, m, of the system where

$$m = \frac{\epsilon}{\sqrt{R_B}}$$

with $R_B$ being the background counting rate and $\epsilon$ being the detection efficiency for carbon-14. The figure of merit is also plotted in Figure 30 where it is seen that in this case the optimum value of amplifier gain for the scintillator is 12, yielding a maximum figure of merit of 3.9.

### 5.2.8 Demonstration of Detection Sensitivity

In Table IX some data are presented for the carbon-14 detection system operated under optimum conditions (viz., SNAP-19 unit viewed end-on at a distance of 1 meter, with 0.47" of tungsten shielding covering the counter). The counter was filled with 33 picocuries of carbon-14, producing a counting rate of 67 cpm, as determined with the SNAP unit removed. The counter was then operated with the SNAP in place, both for this gas sample and for

Table IX. Demonstration of Detection of 33 Picocuries of $^{14}C$ in the Presence of the SNAP-19 Unit Under Optimum Operating Conditions*

| Scint. Coarse Gain | Counts Recorded in 2 Minutes With $^{14}C$ | Without $^{14}C$ | Difference |
|---|---|---|---|
| 16 | 549 | 420 | 129 |
| 32 | 438 | 342 | 96 |
| 64 | 484 | 427 | 57 |

* SNAP-19 unit at $0^{o}$ (end-on), one meter from the counter, with 0.47 inch tungsten shielding over the counter. The figures of merit were determined to be 5.2, 6.2, and 4.4 for scintillator gain settings of 16, 32, and 64, respectively.

a sample containing no carbon-14. As is evident from Table IX, this level of carbon-14 sample was clearly detected under these conditions of exposure to the SNAP-19.

### 5.2.9 Comments on the SNAP-19 Unit

As pointed out in section 5.2.4, the experiments with the SNAP-19 unit clearly demonstrated that the chief interference is due to high energy gamma rays and, presumably, mostly to the 0.76 and 2.61 MeV gamma rays emitted by the SNAP-19. The former gamma ray is emitted by the $^{238}Pu$ fuel and cannot be eliminated. However, the latter gamma ray has been traced to the emissions of the isotope $^{208}Tl$ which arises from the decay of $^{236}Pu$ according to the scheme shown in Table X. It is to be noted that $^{236}Pu$ is present only at a minor trace level (see Table VII); nonetheless, its radiation output is extremely significant. As seen in the decay scheme, the interfering isotope, $^{208}Tl$, grows from the $^{236}Pu$ in a manner chiefly determined by the 2.85-year half-life of this isotope and the 72-year half-life of its daughter, $^{232}U$. During processing of the Pu fuel, much of the uranium impurities are removed. Thus, although it is completely impractical to reduce the $^{236}Pu$ content of the fuel, it is possible to reduce the $^{232}U$ content to a very low level so that the growth of $^{208}Tl$ begins essentially at the end of fuel processing. In Figure 31 a curve showing the growth of this isotope is given to indicate the rapid changes in $^{208}Tl$ level in the first few years after processing. In short, the $^{208}Tl$ content and hence the relative level of the 2.61 MeV gamma ray from the SNAP-19 unit is strongly dependent upon the history of the unit. The shorter the time between fuel processing and use of the unit, the lower will be the high energy gamma ray output.

Table X. Decay Scheme for $^{236}Pu$ and Chief Gamma Emissions of its $^{208}Tl$ Daughter Product

$$^{236}Pu \xrightarrow{2.85\ yr.} {}^{232}U \xrightarrow{72\ yr.} {}^{228}Th \xrightarrow{(1.91\ yr.\ total)} \rightarrow\rightarrow\rightarrow\rightarrow {}^{208}Tl \xrightarrow{3\ min.} {}^{208}Pb$$

(Stable)

$^{208}Tl$ Gamma Rays

| | |
|---|---|
| 2.61 MeV | 100% |
| 0.86 MeV | 12% |
| 0.58 MeV | 86% |
| 0.51 MeV | 23% |

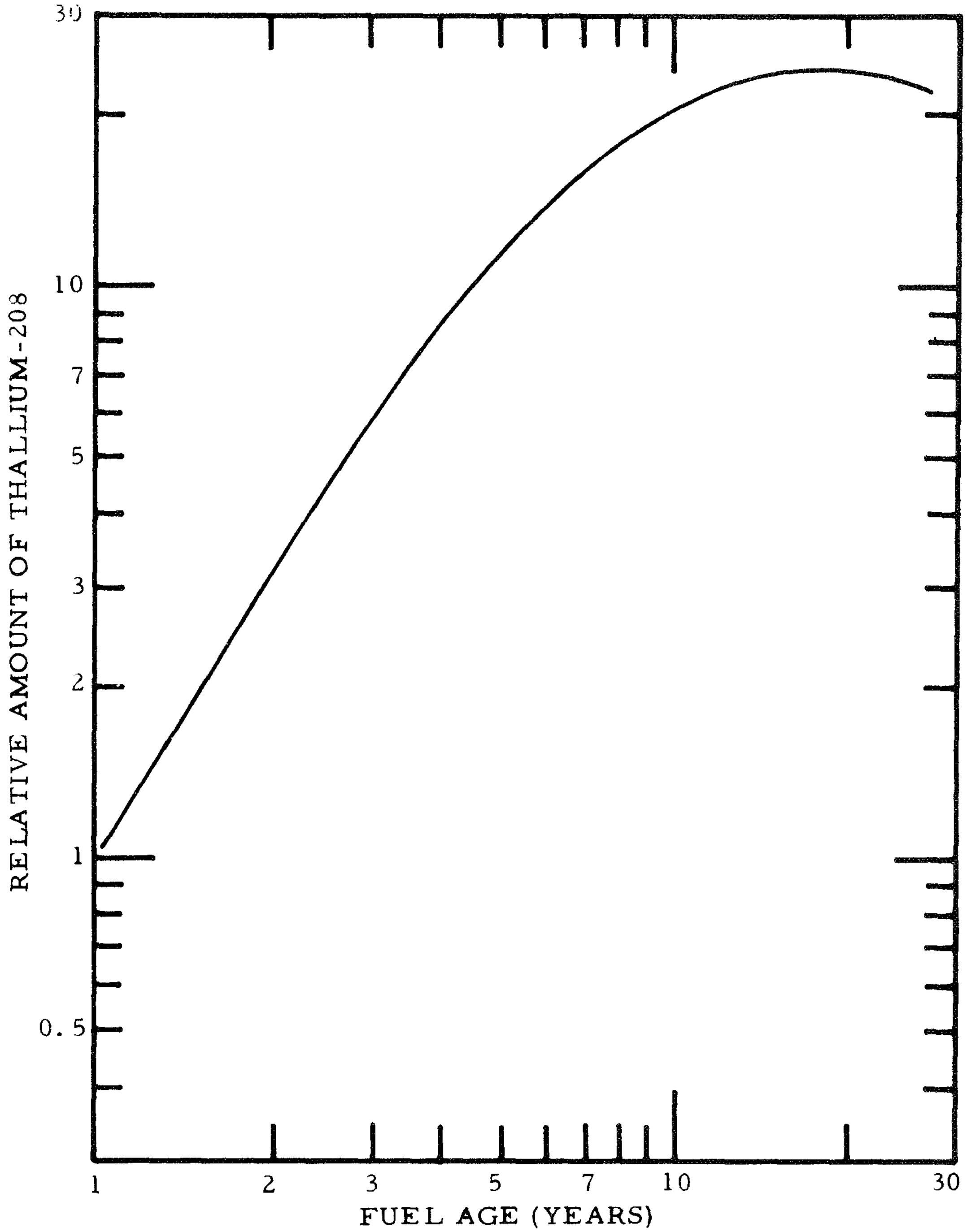


Fig. 31. Growth of the $^{208}$Tl isotope from $^{236}$Pu in SNAP-19 fuel (data provided by Mr. Ed Anderson, Mound Laboratory).

## 6.0 SPECIAL REQUIREMENTS

### 6.1 Power Consumption

It is desirable that the sensors of the radiation detection system require no more than 250 milliwatts of electrical power. As presently constructed, the requirements for power at maximum counting rate are 0.2 milliwatts for the proportional counter, 1200 milliwatts for the photomultiplier tube of system #1, and 150 milliwatts for the photomultiplier tube of system #2. The relatively high power consumption of the photomultiplier tubes is due almost entirely to losses in the resistor network used to bias the dynode structure. For the equipment developed to date, the bias string is made up of 110 K ohm resistors (see Figure 6). The power consumption of the photomultiplier tube could be reduced to a maximum of 120 milliwatts by simply replacing these resistors with 1.1 M ohm resistors which should not interfere with proper operation of the tubes. Thus, no difficulty is expected in optimizing the system for acceptable power consumption. Of special importance is the fact that neither the proportional counter nor the photomultiplier tube requires power supplies of exceptional voltage stability. This is because the counter operates on a very broad, very flat plateau, and because the photomultiplier tube operates only as an anti-coincidence source so that variations in tube gain by a factor of two only slightly affect the figure of merit of the detection system (see Figure 30).

## 6.2 Operating Temperature Range

The design operating temperature range for the detection system is $10^{\circ}C$ to $50^{\circ}C$. The data of Table XI demonstrate the outstanding constancy of the proportional counter counting rate for variations in temperature. This is because the gas gain of a counter is essentially independent of temperature of the counting gas as long as the total amount of gas remains constant. Likewise, the gain change of the photomultiplier tube is expected to be unimportant over this temperature range. In fact, the chief temperature-dependent factor will be the noise of the photomultiplier tube. Since the detection system is designed so that a certain amount of extraneous noise from the tube is tolerated (to maximize sensitivity), no adverse effects due to operating temperature are anticipated for the sensors. It is likely that the electronic systems designed for measuring the outputs of these sensors will be inherently much more sensitive to temperature variations than the sensors themselves.

## 6.3 Sterilization Compatibility

Conventional photomultiplier tubes cannot withstand the $135^{\circ}C$ sterilization qualification temperature specified for the Viking mission. This is because one component of the photocathode, cesium, sublimates throughout the tube at such temperatures. To meet this requirement, a special high-temperature photomultiplier tube with a non-cesiated cathode has been built into one of the detection systems (#1). This tube has performed in every way as satisfactorily as the tube with the cesiated cathode (counter #2). In particular, anti-coincidence effectiveness in the presence of SNAP-19 radiation is equivalent for the two tubes.

Table XI. Stability of Proportional Counter Output to Variations in Operating Temperature. Data taken by exposing a sealed counter containing P-10 gas to $^{137}Cs$ gamma rays with the counter in a temperature-controlled oven.

| Counting Rate (cpm) | Remarks |
|---|---|
| 25, 869 | Oven off. Room temp. is 28°C. |
| 25, 309 | After 10 min. at 30°C. |
| 25, 694 | After 1 hour heating. Oven at 46°C. |
| 25, 652 | 46°C. Turn heat off, open door. |
| 25, 797 | 5 min. later. Air temp. 33°C. |
| 25, 388 | 15 min. later. Air temp. 30°C. |
| 25, 475 | 30 min. later. Air temp. 28°C. |

Tests made by heating a proportional counter to 135°C in an oven showed that the scintillator material, although rated at 160°C by the manufacturer, is not satisfactory, at least in the present configuration. At temperatures above about 90°C this material becomes rubbery and soft. A large amount of sagging occurred at the high temperature limit, completely distorting the spherical counting volume. It is possible that special design and fabrication techniques could provide sufficient support of this material to allow its use at sterilization temperatures. A more promising approach is to investigate the suitability of cesium iodide scintillator for this application. As was pointed out above, this material was not included in the present investigation because of a temporary inavailability of the material in the proper shape. It is believed that further work with the plastic scintillator or use of the cesium iodide will allow complete satisfaction of the requirements for sterilization compatibility.

## 6.4 Operation in the Presence of Water Vapor

Although it is specified that if the detection system is sensitive to water vapor to a deleterious degree, the vapor will be removed by equipment supplied with the life detection system, it is still of interest to test the sensitivity of this instrument to water vapor. The counter has been filled with various quantities of water vapor from 0.25 to 15 Torr mixed with P-10 or 90% Ar-10% $CO_2$ gas. The water was freed of dissolved oxygen by vacuum distillation. The effects noted include a shift of the plateau to higher voltages and a decrease in gas gain as evidenced by a change in signal level from an iron-55 source. The shifts in gas gain never exceeded a factor of 3. Changes in plateau amounted to less than 150 volts. Thus, the consequences were relatively minor. Only at the highest concentration tested did water vapor seriously interfere with normal operation of the counter. This interference was manifested as a partial discharge within the counter. It is highly likely that this was due to condensation of water vapor on the insulator surface. Thus, the counter should be capable of operating in very high humidity atmospheres so long that conditions are such that condensation cannot occur. Similar experiments with oxygen gave similar results. This greatly extends the usefulness of this detection system in connection with other life detection system requirements.

## 7.0 REFERENCES AND BIBLIOGRAPHY


Be-68 P. W. Benjamin, C. D. Kemshall, and J. Redfearn, "A High Resolution Spherical Proportional Counter", Nucl. Instr. Meth. 59 (1968) 77.

Bl-68 S. Block, C. T. Schmidt, and R. L. Kathren, "Radiation Dosimetry and Spectral Distribution of the SNAP-19 Source", UCRL-50539 (Nov., 1968).

Bo-67 D. D. Bockman, D. C. Brandt, and A. L. Babb, "The Solubility of $CO_2$ in a Solution of Phosphors in Polyvinyltoluene", Int. J. Appl. Rad. Isotopes 18 (1967) 728.

Cl-69 B. C. Clark and W. Gross, "Limitations of Commercial Krypton for Proportional Counting", Rev. Sci. Instr. 40 (1969) 504.

Cu-65 S. C. Curran and H. W. Wilson, "Proportional Counters and Pulse Ion Chambers", in Alpha-, Beta-, and Gamma-Ray Spectroscopy, Ed. by K. Siegbahn, North-Holland Pub. Co., Amsterdam (1965).

Em-66 E. W. Emery, "Geiger-Mueller and Proportional Counters" in Radiation Dosimetry II, Ed. by F. H. Attix and W. C. Roesch, Academic Press, N. Y. (1966).

Ev-55 R. D. Evans, The Atomic Nucleus, McGraw-Hill Book Co., Inc. (1955).

Fr-62 W. Franzen and L. W. Cochran, "Pulse Ionization Chambers and Proportional Counters", in Nuclear Instruments, Ed. by A. H. Snell, John Wiley and Sons, N. Y. (1962)

Gr-57 G. W. Grodstein, "X-Ray Attenuation Coefficients from 10 keV to 100 MeV", U.S. Nat'l. Bur. Std. Circular 583 (1957)

Hu-67 B. Huber, F. Heinrich, H. Von Buttlar, "A Low-level Gas Counter with a Plastic Scintillator as Anti-coincidence Shield", Nucl. Instr. Meth. 52 (1967) 104.

Ka-69 R. A. Kaminskas, G. W. Ryan, C. A. Smith, "RTG/Science Instrument Radiation Interactions for Deep Space Probes", Phase I Report, Contract NAS 2-5222 to NASA/Ames (July, 1969).

Ne-58 A. T. Nelms, "Energy Loss and Range of Electrons", U.S. Nat'l. Bur. Std. Supplement to Circular 577 (1958).

Wa-64 D. E. Watt and D. Ramsden, High Sensitivity Counting Techniques, The MacMillan Co., N. Y. (1964).

We-64 W. R. Weber, "A Survey of Solar Flare Data", Boeing Document D2-90469 (1964).

Wi-61 R. W. Williams, "Gas-Filled Counters", in Methods of Experimental Physics V, Ed. by L. C. L. Yuan and C. Wu, Academic Press, N. Y. (1961).

## 8.0 CONCLUSIONS AND RECOMMENDATIONS

The most important conclusion that can be drawn from the present investigation is that the present approach to the carbon-14 detection problem is not only feasible, but is capable of meeting or surpassing nearly every design goal set for this measurement. The ability of this system to reject interfering radiation from cosmic rays, solar flares, natural radioactivity, and the radiation from radioisotope thermoelectric generators is outstanding, with rejection factors varying from 15 to 60 for gamma radiation and being theoretically much higher for charged particle radiation. At the same time the detection system is capable of measuring the carbon-14 radiation with an efficiency between 40 and 95%, depending on the conditions for background rejection. It has been demonstrated that the counter can operate satisfactorily over wide ranges of temperature, gas pressure, and gas composition, and in the presence of water vapor or oxygen in relatively high concentrations. The developed system exhibits a high percentage of live volume, a very wide dynamic range, and excellent sensitivity to low levels of carbon-14. The unit operates well at any orientation with respect to the external radiation sources, e.g., the RTG's. The reproducibility and long term stability of the system is excellent.

### 8.1 Reducing Interference from the RTG's

Experiments conducted with the SNAP-19 unit to simulate the RTG radiation has produced information leading to the following recommendations:

1. The carbon-14 system should be located approximately equidistant from the two SNAP units.

2. As much material as possible should be placed between the detection system and the two SNAP units. This may be accomplished by judicious layout of experiments.

3. If possible, the RTG units should be oriented so that the SNAP power sources are in end-on configuration as viewed by the carbon-14 detection system.

4. Procedures should be established to guarantee that the fuel used in the SNAP units will be as "young" as is feasible when installed on the Lander to minimize $^{208}Tl$ radiation.

With respect to items 1 and 3 above, Figure 32 is provided to show the consequences of not satisfying these recommendations. In the first part of this figure, variations in background counting rate are calculated assuming that the detection system is to be located on a line between two SNAP units which are 200 cm apart. The mid-point is the preferred location, although variations of distance of 20 to 30 cm around this position are not crucial. The second part of this figure gives the dramatic variation in background due to different orientations of the SNAP units.

## 8.2 Future Areas of Study

Although this investigation has succeeded in answering a host of questions concerning this basic approach and has produced the data required to verify its feasibility, it has likewise brought out areas requiring further study for development of this device to the point

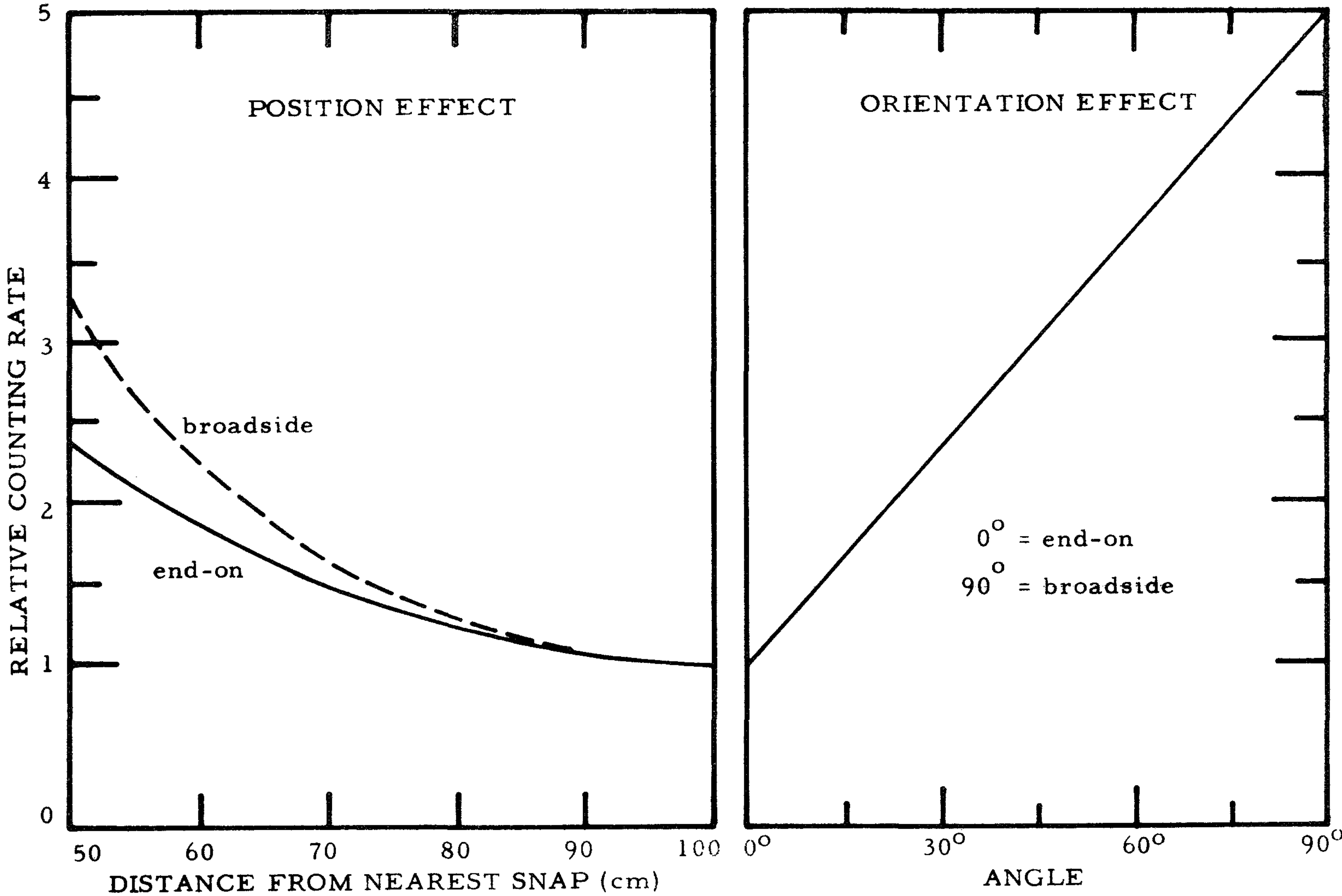


Fig. 32. Summary of background counting rate as a function of distance from each of two SNAP-19 units separated by 200 cm and as a function of the orientation angle of the SNAP-19 units.

from which flightworthy hardware can be fabricated. Thus, the following tasks are recommended for further consideration:

1. Investigate the use of cesium iodide scintillator material and study its properties with respect to heat resistance, gas absorption, and anti-coincidence effectiveness.

2. Evaluate the use of a flight-qualified photomultiplier tube (Johnston Laboratories Model P-10) in this system, including its effect upon anti-coincidence effectiveness.

3. Extend the usefulness of this technique to other life detection methods by in-depth investigations of the effects of oxygen, water vapor, and other gases upon the operating characteristics and the carbon-14 detection sensitivity of the system.

4. Perform studies designed to extend the dynamic range of the present system to higher levels of carbon-14 detection.

5. Design the system for ruggedness and minimum weight; fabricate a prototype and conduct suitable studies to determine the flight-worthiness of the design.

6. Determine the specifications for flight hardware (sensitivity, temperature dependence, accuracy, etc.)

## APPENDIX A

### Mathematical Derivation of Minimum Detection Limits and the Figure of Merit

Define the quantities:

$R_S$ = counting rate (cpm) of the $^{14}C$ sample alone

$R_B$ = background counting rate (cpm)

$R_{SB}$ = total counting rate when $^{14}C$ is in the counter (cpm)

$t$ = time for counting background = time for counting $^{14}C$ sample (minutes)

$A$ = $^{14}C$ sample activity (dpm)

$\epsilon$ = counter detection efficiency for $^{14}C$ (per cent)

$\sigma$ = standard deviation of the count obtained

It follows at once:

$$R_{SB} = R_S + R_B \tag{1}$$

$$R_S = 0.01\ \epsilon\ A \tag{2}$$

$$\sigma_B = \sqrt{R_B t} \tag{3}$$

$$\sigma_{SB} = \sqrt{R_{SB} t} \tag{4}$$

$$\sigma_S = \sqrt{\sigma_B^2 + \sigma_{SB}^2} = \sqrt{R_B t + R_{SB} t}$$

$$= \sqrt{(R_S + 2\ R_B)\ t} \tag{5}$$

To find the minimum level of activity of $^{14}C$ which can be detected by this counter, A(min), assume this level must produce a counting rate, $R_{SB}$(min), which gives a count in time t which is greater than the background count that would be obtained over an identical length of time by an amount $\alpha$ times the standard deviation of the background count ($\alpha$ is arbitrary for the time being):

$$R_{SB}(\text{min})\, t = R_B t + \alpha \sigma_B \qquad (6)$$

Applying Eq. (1) and (3) to this equation, one can show

$$R_S(\text{min}) = \alpha \sqrt{\frac{R_B}{t}} \qquad (7)$$

Through Eq. (2) we transform to

$$A(\text{min}) = \frac{100\alpha}{\sqrt{t}} \left( \frac{\sqrt{R_B}}{\epsilon} \right) \qquad (8)$$

The quantity in parentheses can be defined as:

$$m = \frac{\epsilon}{\sqrt{R_B}} = \text{figure of merit of the counter} \qquad (9)$$

so that Eq. (8) becomes

$$A(\text{min}) = \frac{100\alpha}{m\sqrt{t}} \qquad (10)$$

Use of the quantity m is very convenient in determining the optimum conditions for operating a counter and for comparing and evaluating different $^{14}CO_2$ detection systems. The larger the m, the better the system. A counter which has a figure of merit 3 times higher than that of another counter can detect a 3 times lower level of radioactivity, and hence a 3 times lower level of life. The value of m also determines the accuracy to which the $^{14}C$ activity can be determined when the background counting rate is high. This can be shown by calculating the relative standard deviation of the activity, $r_A$

$$r_A = \frac{\sigma_A}{A} = \frac{\sigma_S}{R_S t} \tag{11}$$

(Note: Relative standard deviation is also known as "fractional standard deviation", and "coefficient of variation".) Combining Eq. (2), (5), and (9) with Eq. (11), one finds

$$r_A = \left(\frac{10}{\sqrt{At}}\right) \sqrt{\frac{1}{\epsilon} + \frac{200}{m^2 A}} \tag{12}$$

It is instructive to examine this equation for two cases:

a) low sample activity ($R_S \ll 2\,R_B$), where it can be shown

$$r_A \simeq \frac{141.4}{mA\sqrt{t}} \tag{13}$$

b) high sample activity ($R_S \gg 2\,R_B$), where it can be shown

$$r_A \simeq \frac{10}{\sqrt{\epsilon At}} \tag{14}$$

Thus, for a weak $^{14}C$ sample, the accuracy to which the measurement can be made is determined solely by the figure of merit, the level of activity, and the time allotted to the count. In contrast, at high sample strengths, the detection efficiency replaces the figure of merit as the determining factor.

The use of Eq. (10) and (13) to calculate the minimum detection limit and minimum relative standard deviation requires knowledge of the instrumental figure of merit, m, selection of counting time, t, and a value of $\alpha$. To assist in the latter, Table A-I has been prepared to give the values of required to place confidence levels of up to 0.999999 that the observation of the count given in Eq. (6) is not simply due to statistical fluctuations of background.

Table A-1. Probability of observing a count more than $\alpha$ standard deviations above the mean count (assumes a normal distribution).

| $\alpha$ | Probability |
|---|---|
| 1.28 | $10^{-1}$ |
| 2.33 | $10^{-2}$ |
| 3.09 | $10^{-3}$ |
| 3.72 | $10^{-4}$ |
| 4.26 | $10^{-5}$ |
| 4.76 | $10^{-6}$ |